

Ionic Liquid and Lithium Salt Mixtures as Ionic Sources

by

Maria Regina Apodaca Moreno

Submitted to the Department of Aeronautics and Astronautics
in partial fulfillment of the requirements for the degree of
Masters of Science in Aeronautical and Astronautical Engineering

at the

MASSACHUSETTS INSTITUTE OF TECHNOLOGY

September 2020

© Massachusetts Institute of Technology 2020. All rights reserved.

Author
Department of Aeronautics and Astronautics
May 19, 2020

Certified by
Paulo Lozano
Professor
Thesis Supervisor

Accepted by
Sertac Karaman
Chairman, Department Committee on Graduate Theses

Ionic Liquid and Lithium Salt Mixtures as Ionic Sources

by

Maria Regina Apodaca Moreno

Submitted to the Department of Aeronautics and Astronautics
on May 19, 2020, in partial fulfillment of the
requirements for the degree of
Masters of Science in Aeronautical and Astronautical Engineering

Abstract

Ionic liquids (ILs) are molten salts that are used in electrospray thrusters as the source for the ionic emission. The total current of the emitted ions is proportional to the conductivity and the surface tension of the ionic liquid. Since the thrust of the propulsion system is dependent on the current, we try to maximize the total current emitted. However, the production of new ionic liquids is very challenging and thus this thesis explores the use of mixtures as an alternative ionic source. This thesis studies the relationship that exists between temperature, conductivity and surface tension with the concentration of $LiBF_4$ salt in the $EMIBF_4$ ionic liquid. The solvent was selected given it is one of the most commonly used ionic liquids in electrospray propulsion. The salt, on the other hand, was selected because of its small and simple positive ion Li^+ and its matching negative ion, BF_4^- to that of the IL. From measurements at a concentration of 27wt% time of flight spectrometer, an increase in the percentage of the beam that was single EMI^+ from $\sim 50\%$ to $\sim 70\%$. This lead to an increase in efficiency of $\sim 2\%$ and specific impulse of $\sim 27\%$. It was found that the surface tension of the mixture decreases as the concentration increases. Likewise, the conductivity tends to decrease as the weight percentage of salt is increased, except for a local maximum around 15wt%.

Thesis Supervisor: Paulo Lozano
Title: Professor

Acknowledgments

First and foremost I would like to thank my advisor Prof. Paulo Lozano. Profe, you gave me this amazing opportunity to be part of such an great lab and for that, I am extremely grateful. The knowledge and the people I interacted with during my time here, have changed and shaped my future for the better.

Secondly, I would like to thank everyone who helped make this project possible. PhD. Catherine Miller, thank you for teaching me the ropes of the lab, as well as providing crucial results for this thesis. Tom Coles, thank you for teaching me how to do MD simulations, I know my learning curve was not ideal. Thank you Todd Billings for your patience and advice everytime I would go down to the machine shop. Naylah Canty, thank you so much for your help doing some of the experiments in this thesis. You were a great UROP and I believe you have a bright future ahead of you.

Thirdly, I would like to thank everyone in SPL. Ximo, the compassion and empathy you should me, makes me certain you will make a great professor one day. Elaine, you have truly shown me not to lose faith in academia because there are professors like you looking to, not only out conspiracy theories, but also change a broken system. Mia, thank you for constantly reminding me that we just work here. Colin, Andrew, Yiyun, and Oli, your friendship and coffee breaks made SPL the fun and welcoming lab it is. Jon, you kept me sane and grounded since the day we met. Without FGC, MIT would have been impossible. Faisal, your energy and belief, brought out the best in me. Dani, your constant emotional support really helped me navigate my life as a grad student. Rumya, thank you for helping me find my home away from home.

Laslty, I would like to thank my family. A mi abuelita, tía y mamá, gracias por siempre ser mis ejemplos a seguir. En la vida, pocas veces tuve miedo a caer porque siempre las tuve de apoyo. Eva y Sofia, nunca pense que las extrañaría tanto, aunque esté lejos, siempre están conmigo.

This research would not have been possible without the financial support from Sandia National Laboratories and Lic. Miguel Alemán Velasco.



Contents

1	Introduction and Background	15
2	Literature Review	19
2.1	Ionic Liquids	19
2.2	Mixtures	21
2.3	Electrosprays	23
2.4	Fragmentation and Droplet effects	24
3	Experimental Methods	29
3.1	Single Tip Manufacturing	29
3.2	Surface Tension Experiments	32
3.2.1	Setup	33
3.3	Temperature vs. Conductivity	34
3.3.1	Setup	34
3.4	Retarding Potential Analyzer Experiments	35
3.4.1	Setup	37
3.5	Time of Flight Mass Spectrometry Experiments	38
3.5.1	Setup	39
4	Molecular Dynamics Simulations	41
4.1	Theory	41
4.2	Selected Properties.	42

5	Results and Discussion	45
5.1	Surface Tension Results	45
5.2	Temperature vs. Conductivity Results	46
5.3	Time of Flight Results	49
5.4	Simulations	54
5.5	RPA Results	54
6	Conclusion and Future Work	57
6.1	Conclusions	57
6.2	Experimental Future Work	58
6.3	Simulations Future Work	59
A	Individual Conductivity vs. wt% at constant Temperature Graphs	61
B	Individual Conductivity vs. Temperature at constant wt% Graphs	69
C	Colour Changes Due To Temperature Experiments	73

List of Figures

2-1	Example of the neutral molecules of the ionic liquid use as the solvent and the solid salt of the mixtures referred to in this thesis.	22
2-2	Diagram of an electrospray thruster.	24
3-1	First two out of the five components that composed the single emitter tip setup designed for this thesis.	31
3-2	Components to the single emitter tip setup.	31
3-3	Picture of the complete single emitter tip setup mounted on the the vacuum chamber with the necessary connections.	32
3-4	Example of a liquid drop on clean microscope slide.	33
3-5	Example of a liquid column up a capillary tube.	34
3-6	Picture of the heating setup. On the left there is the heating plate, the dry box connected to the nitrogen and the conductivity meter probe. On the right, is the conductivity meter.	35
3-7	Idealized RPA curves.[16]	36
3-8	Picture of the spherical RPA setup designed by Catherine Miller. [16]	37
3-9	Idealized ToF curves.[16]	39
3-10	Picture of the ToF setup designed by Catherine Miller. [16]	40
4-1	Example of a $EMIBF_4 + 27wt\%LiBF_4$ 15nm droplet with 720 neutral pairs.	42
5-1	Surface Tension vs the salt weight percentage in the mixture at a constant $25^\circ C$	46

5-2	Conductivity vs Temperature in C at constant $LiBF_4$ wt%.	47
5-3	Conductivity vs $LiBF_4$ wt% at constant Temperatures in C.	48
5-4	Comparison of heat-up and cool-down conductivity vs. temperature curves for multiple mixtures.	49
5-5	Normalized current vs mass, ToF graph produced by Catherine Miller, for both the pure $EMIBF_4$ ionic liquid (blue curve) and the mixture of this same liquid with 27wt% of $LiBF_4$ salt (red curve).	50
5-6	Normalized Current vs Normalized Voltage for pure $EMIBF_4$ ionic liquid.	55
A-1	Conductivity vs. wt% at a constant temperature of 25°C	61
A-2	Conductivity vs. wt% at a constant temperature of 27°C	62
A-3	Conductivity vs. wt% at a constant temperature of 30°C	62
A-4	Conductivity vs. wt% at a constant temperature of 33°C	62
A-5	Conductivity vs. wt% at a constant temperature of 35°C	63
A-6	Conductivity vs. wt% at a constant temperature of 37°C	63
A-7	Conductivity vs. wt% at a constant temperature of 40°C	63
A-8	Conductivity vs. wt% at a constant temperature of 43°C	64
A-9	Conductivity vs. wt% at a constant temperature of 45°C	64
A-10	Conductivity vs. wt% at a constant temperature of 47°C	64
A-11	Conductivity vs. wt% at a constant temperature of 50°C	64
A-12	Conductivity vs. wt% at a constant temperature of 53°C	65
A-13	Conductivity vs. wt% at a constant temperature of 55°C	65
A-14	Conductivity vs. wt% at a constant temperature of 57°C	65
A-15	Conductivity vs. wt% at a constant temperature of 60°C	66
A-16	Conductivity vs. wt% at a constant temperature of 63°C	66
A-17	Conductivity vs. wt% at a constant temperature of 65°C	66
A-18	Conductivity vs. wt% at a constant temperature of 67°C	67
A-19	Conductivity vs. wt% at a constant temperature of 70°C	67
A-20	Conductivity vs. wt% at a constant temperature of 73°C	67

A-21	Conductivity vs. wt% at a constant temperature of 75°C	68
A-22	Conductivity vs. wt% at a constant temperature of 77°C	68
A-23	Conductivity vs. wt% at a constant temperature of 80°C	68
B-1	Conductivity vs. T at a constant mixture with no $LiBF_4$ salt	69
B-2	Conductivity vs. T at a constant mixture with 2.5wt% of $LiBF_4$ salt.	70
B-3	Conductivity vs. T at a constant mixture with 5wt% of $LiBF_4$ salt.	70
B-4	Conductivity vs. T at a constant mixture with 7.5wt% of $LiBF_4$ salt.	70
B-5	Conductivity vs. T at a constant mixture with 10wt% of $LiBF_4$ salt.	71
B-6	Conductivity vs. T at a constant mixture with 15wt% of $LiBF_4$ salt.	71
B-7	Conductivity vs. T at a constant mixture with 20wt% of $LiBF_4$ salt.	71
B-8	Conductivity vs. T at a constant mixture with 25wt% of $LiBF_4$ salt.	72
B-9	Conductivity vs. T at a constant mixture with 30wt% of $LiBF_4$ salt.	72

List of Tables

4.1	Matrix of the properties selected for the different simulations run. The second column are the values of the electric field applied to the simulation. These were all along the x-axis. The third column are the number of total neutral pairs that make up the initial droplet. Lastly, the fourth column is the total real time that has been simulated. All runs were done at a constant temperature of 300 K.	43
5.1	Beam composition breakdown for the pure $EMIBF_4$ ionic liquid ToF. The values were obtained by measuring the heights of the different steps of the pure ionic liquid curve in figure 5-5	51
5.2	Beam composition breakdown for the $EMIBF_4$ ionic liquid mixed with 27wt% of $LiBF_4$ ToF measurements. The values were obtained by measuring the heights of the different steps of the curve of the 27wt% of $LiBF_4$ mixture, figure 5-5	51
5.3	Efficiency values for the pure ionic liquid $EMIBF_4$ and the mixture of this same liquid with 27wt% of $LiBF_4$ salt. These values were extracted from the ToF graph (figure 5-5).	51
5.4	Selected 2 species, beam composition percentage and mass of ions for the $EMIBF_4$ ionic liquid and for the 27wt% $LiBF_4$ mixture, taken from the ToF measurements (figure 5-5)	52

5.5	Efficiency values for the pure ionic liquid $EMIBF_4$ and the mixture of this same liquid with 27wt% of $LiBF_4$ salt. These values were extracted from the ToF graph (figure 5-5) and using the 2 species approximation (see equation 5.3).	52
5.6	I_{sp} reduction calculated using both the 2 species approximation (see equation 5.3) and the integration method (see equation 2.24).	53
5.7	Results obtained from different simulation.	54
C.1	Colour change after heating mixtures.	73

Chapter 1

Introduction and Background

Up until now, most of the research and characterization has been done for pure ionic liquids. Their surface tension, conductivity and emission properties have been carefully studied and documented by multiple authors. However, there is little research in the field when it comes to the previously mentioned properties in a mixture [1], let alone a highly asymmetrical mixture as the one used in this thesis. By adding a salt to a pure ionic liquid, we add an additional variable of concentration that opens the door to multiple new questions. The main reasoning behind the study of mixtures is not only to push the boundary of our understanding of how such mixtures would act in given circumstances, but also to improve the performance of one of its possible applications: electrospray propulsion. Electrospray propulsion is based on the emission of charged particles that are extracted, from an ionic source, and accelerated by an electrostatic field. Electrospray thrusters use ionic liquids as the ionic sources for their emission. In general, the production and development of these liquids are a lot more complicated than the simple mixing process that is done in this work. Therefore, the results of this thesis could provide a simple alternative for performance improvement. This performance improvement can be measured by seeing an increase in specific impulse and by decreasing the polydispersity of the beam. Polydispersity is the presence of species of different masses in the beam. This polydispersive effect causes a loss in efficiency of the propulsion system since the total power that is being used to accelerate all ions is the same but the energies reached by each species are not. The current

state of the art suggests that this increase in performance is dependent on properties of the liquids such as: surface tension, conductivity, amongst others, that can be changed by the addition of salts. This leads to the main goal of this thesis to be the measuring and characterization of mixture between a commonly used ionic liquid $EMIBF_4$ and the salt $LiBF_4$ at different weight percentages and temperatures. The goal is to find the concentration that has the desired properties leading to the highest increase in performance. The main reasoning behind the selection of the salt is its small and simple positive ion Li^+ and the matching negative ion BF_4 to that of the solvent. The hopes of this thesis is to see an increase in emission of single Li^+ ions since they are the lightest ions and therefore would reach higher velocities leading to higher thrust.

Ongoing research in the field has also proven a lack of standardization in methodology when it comes to the characterization of both ionic liquids and mixtures. Making this the second goal of this thesis to characterize the new mixtures in the same way that ionic liquids have in the past. The methodology used in this thesis in order to characterize the mixture is using the same instruments and similar experimental setup as the ones used to study pure ionic liquids. These instruments include a spherical retarding potential analyzer, to characterize the energy distribution of the beam, and a time of flight mass spectrometer, to study the mass distribution of the beam. [16] However, since the mixtures are made in house, additional experimental setups had to be designed in order to further characterize the mixtures properties. These experiments consisted of the testing of the surface tension of the mixtures, as well as the conductivity at different temperatures. Additional steps in handling and preparation were taken in order to ensure that the humidity of the environment was not being absorbed by the mixtures and therefore changing their chemical and physical properties.

The third goal of this thesis is to have a better understanding of what is happening at a molecular level. This lead to the inclusion of molecular dynamics simulations. These simulations were done based on a code that was previously written by Ph.D candidate Tom Coles, and was modified by the author of this thesis to simulate

the mixtures and concentrations studied in this work. By comparing simulations to experiments, it would be possible to validate the findings. The inclusion of simulations can help make a better informed decision of what can be expected to be a good mixture and at what temperature and concentration, the desired results can be obtained.

Chapter 2

Literature Review

The work that has been done up until now regarding ionic liquids, used in electric propulsion, has been limited to single ionic liquids and the effects different field geometries may have in their performance. However, this thesis aims to focus on the possibility of using mixtures as ion sources. This opens several questions to how mixtures will interact under similar conditions to the "pure" ionic liquids. In order to see the contribution to the field of this thesis, one must first define what ionic liquids are, how they differ from mixtures, what role they play in electrospray propulsion and what is the issue that is being address by making this change.

2.1 Ionic Liquids

Ionic liquids (ILs) are salts that are found in the liquid form at temperatures below $100^{\circ}C$. They consist of both positive and negative molecules that allow the liquid to interact with an external electric field. Their ion mobility allows for the transportation of current. Unlike most organics solvents, i.e. water, that are kept together via Van Der Waals forces, the molecules that form ionic liquids are tied together through Coulomb forces. Ionic liquids are known to have negligible vapor temperature, a wide electro-chemical window, high thermal and chemical stability, and highly significant ionic conductivity. These physical and chemical properties are what make them very attractive to different fields. They were first synthesized by Walden in 1914.[24]

Since then, many different kinds of ionic liquids have been developed for a variety of applications such as solvents for organic synthesis and catalysis, as electrolytes for batteries [11] and as ionic sources for electrospray propulsion. For the purpose of this thesis, the characteristics that shall be further explored are those that benefit electrospray propulsion.[13]

Conductivity is probably the most important property for the use of ILs in electrospray propulsion. In a molten salt, conductivity can be described as:

$$\sigma = \frac{yF^2d}{6\pi N_A FW \eta} [(\zeta_a r_a)^{-1} + (\zeta_c r_c)^{-1}] \quad (2.1)$$

where y is a concentration constant, F is the drag force, N_A is Avogadro's number, d is the density, FW is the formula weight, η is the viscosity, r_a and r_c are the radii of the anion and cation respectively, and finally ζ_a and ζ_c are their microviscosity factors.[2] From this equation, it is possible to see the role both the viscosity of the liquid and the size of the ions play in increasing the conductivity. Therefore, if a higher conductivity is desired, it is necessary to find the IL that has low viscosity as well as small ions.

When an ionic liquid is placed in an electric field, the freedom that the charged molecules have, given its molten state, allows them to rearrange themselves. Due to the presence of the field, charges relax to the surface and form a surface charge density on which a field can act to reform the surface shape. Depending on the polarity of the electric field they are placed in, either the positive or the negative charged molecules will move towards the surface of the liquid. If the field is stronger than a critical value (the activation energy, free energy of a solvation, etc), then ion evaporation could occur. Ionic emission is a carefully experimentally characterized phenomena that has been studied by multiple authors.

Lastly, a very important property that ILs have is their ability to solubilize salts. This opens the door to the main subjects of research of this thesis, mixtures.[2]

2.2 Mixtures

Mixtures are the main focus and novel part of this thesis. When referring to a mixture throughout this thesis, it is between an ionic liquid, which has been defined in the previous section, and a solid salt.

The selection of the two components of the mixture were based on the possible application in electrospray propulsion. This is why, for the solvent, one of the most commonly used ionic liquids was selected: 1-Ethyl-3-Methylimidazolium tetrafluoroborate ($EMI - BF_4$) (see figure 2-1a). The positive molecules ($[EMI]^+$) of this ionic liquid are very complex, i.e. heavy, making them not ideal as having a single atom as the positive ion. As a result, the selected salt had the lightest positive single atom, Lithium (Li^+). The reason why a lithium based pure ionic liquid was not selected is carefully explored by Hitoshi Shobukawa et al[20]. In this paper, they found that lithium ionic liquids have too high of a viscosity, causing their conductivity to be less than ideal. Their viscosity laid between 300 to 1200 $mPas$, making them 10 times higher than those of the typical ionic liquids, while their conductivity was only between $10^{-4} Scm^{-1}$ and $10^{-5} Scm^{-1}$ at $30^\circ C$, two full orders of magnitude less.

The salt that is used in this thesis is lithium tetrafluoroborate ($LiBF_4$) (see figure 2-1b). It is important to keep in mind that the selection of the solvent will affect the ability of extracting the Li^+ from the mixture, as was found by Alexander M. Smith and Susan Perkin.[21] In their paper, they test the extraction and layering structure of the mixture using 2 different solvents, 1-ethyl-3-methylimidazolium bis[(trifluoromethane)sulfonyl]imide ($[C_2C_1Im][NTf_2]$) and 1-ethyl-3-methylimidazolium bis(uorosulfonyl)-imide ($[C_2C_1Im][N(SO_2F)_2]$) but with a single salt lithium bis[(trifluoromethane)-sulfonyl]imide $LiNTf_2$. It was found that one of the solvents, $[C_2C_1Im][NTf_2]$, created a negative cluster around the Li^+ ion preventing it from reaching the surface of the liquid. They attributed this preference to a lower energy of formation for these clusters around the lithium ion versus that of the positive ion of the solvent, $[C_2C_1Im]^+$. The results were completely turned when using the other solvent, $[C_2C_1Im][N(SO_2F)_2]$. No clus-

tering around the Li^+ ion was observed, particularly at higher salt concentrations. This paper concluded that the selection of the solvent was of upmost importance in order to optimise the Li^+ emission. Furthermore, Hayamizu et al.[7]found that with mixtures with $EMIBF_4$ and $LiBF_4$ it is to be expected to see more complex ions at higher concentration. They attribute this property to the reduction in attraction between the EMI^+ and the BF_4^- leading to more free EMI^+ . Another important conclusion to point out from this paper is that there is an increase in effective lithium ion mobility as the temperature of the mixture is increased. The results found by this thesis are somewhat different to those found by Hayamizu et al. [7].

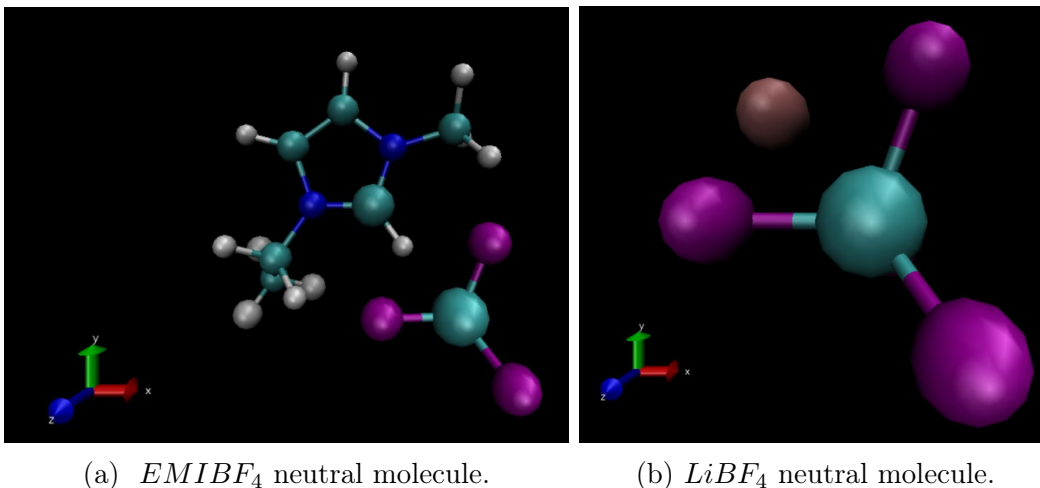


Figure 2-1: Example of the neutral molecules of the ionic liquid use as the solvent and the solid salt of the mixtures referred to in this thesis.

Additionally, it is important to point out the role that the BF_4^- ion plays in the selected ionic liquid. Its geometry, symmetry and molar mass, similarly to other anions, have proven to have a strong influence on the viscosity of IL, and thus the selected ion is highly beneficial to the goal of this thesis. Furthermore, hydrophilic anions, such as BF_4^- , cause a huge change in the liquid's physical properties. A lot of previous work done in the ionic liquid and their mixtures do not always mention the drying procedures that were used to ensure the purity of the liquid. That is why throughout this thesis both the salts and the IL are dried and maintained in dry atmospheres.[8]

Previous simulation studies of Ionic Liquid/Lithium Salt point to their being a

general decrease in ion conductivity of the mixture due to both an increase in viscosity and the formation of clusters. Moreover, it was noted that high ionic conductivity does not necessarily mean high Li^+ motion. When graphing the conductivity due to Li^+ versus the salt concentration, they realised that at a temperature of approximately $25^\circ C$, there was a maximum at $\sim 13mol\%$. This opens the question of whether there is an optimal salt concentration[12].

2.3 Electrospays

Electrospray propulsion is based on a multi-physics problem that consists of both electrostatic theory and fluid dynamics. The motion of the system comes from the emission of ions provided by an ionic liquid. The process of emission is achieved by allowing the ionic liquid to flow through a conductive capillary tube which, if placed in a strong enough electric field, produces what is known as a Taylor Cone.[23] The tip of the cone serves as a singularity point from which the ions are emitted. In practice, an electrospray propulsion system (figure 2-2) consists of thousands of these capillary tubes by using highly porous materials to produce their emitters. The shape of the emitter is very important since the emitter is used as the anode or the cathode of the electrostatic field. The other anode is the extractor grid. The extractor grid, as the name suggest is a metal plate that has holes in order to allow the ions that are being extracted from the liquid to pass and therefor leave the propulsion system. Both the spacing between these and their shapes, determine the strength and geometry of the field, with the main limitation to the design being the arcing voltage at a given atmosphere. Generally, the field that is applied is around the order of $10^6 V/m$, meanwhile at the tip, the electric field is approximately $10^9 V/m$. The current state of the art allows for the production of emitter chips that have several hundreds of tips in a $1cm^2$ square.

The main advantage of electrospray thrusters is their promise of high efficiency. There are two important applications for this type of thrusters: highly precise thrust maneuvers and, given their compact size, as propulsion systems on cubesat missions.[4]

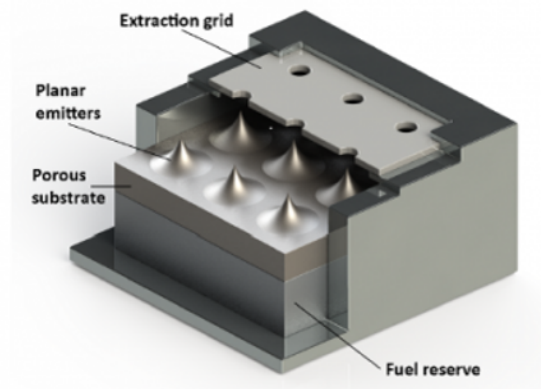


Figure 2-2: Diagram of an electro spray thruster.

2.4 Fragmentation and Droplet effects

Having a purely ionic emission from the Taylor cone in practice is very challenging and thus we occasionally get droplets. These droplets are a lot heavier than single ions and their charge does not scale accordingly. This means that they will not be able to reach great speeds and thus reduce the efficiency in terms of the specific impulse of our system. Specific impulse is defined as:

$$I_{sp} = \frac{F}{\dot{m}g}, \quad (2.2)$$

where F is the thrust of the propulsion system, \dot{m} is the mass flow of the propellant and g is the value of gravity. That is why, previous work done on ionic liquids has been in identifying ionic liquids that are more likely to emit in a purely ionic regime. However, it is important to point out that even in the purely ionic-regime, we experience something known as fragmentation. Fragmentation is when you get conglomerates of positive or negative molecules, along with one or more neutral molecules, that eventually break into smaller ions such as a monomer and a neutral, for example. This is different than droplets because, although they are of greater mass than a single charged molecule at the beginning, they then break into comparable masses. Yet, the droplets can also experience fragmentation and the effect could be stronger. This effect also causes a decrease in efficiency that is dependent on where this fragmentation

occurs. Moreover, having to accelerate ions and clusters of different masses causes an additional efficiency loss. This is known as the polydispersive effect. This efficiency loss comes from needing to apply the same amount of energy to accelerate a mass that will not provide the same amount of thrust to the system since it will not reach the high velocity of the lighter ions. In other words, given the same potential difference, if there are ions of different masses m_j and charges q_j , their velocities would be:

$$c_j = \sqrt{\frac{2q_j V}{m_j}} \quad (2.3)$$

Now, if \dot{N}_j is the number of ions with mass m_j per unit of time, then the total mass flow is defined as:

$$\dot{m} = \sum_j \dot{N}_j m_j. \quad (2.4)$$

Likewise, the total current would be:

$$I = \sum_j \dot{N}_j q_j. \quad (2.5)$$

Since the thrust can be defined as:

$$F = \dot{m} c \quad (2.6)$$

then by inserting equations 2.3 and 2.4, it can be rewritten as:

$$F = \sum_j \dot{N}_j m_j c_j = \sum_j \dot{N}_j \sqrt{2q_j V m_j}. \quad (2.7)$$

On the other hand, it is known that the efficiency of a propulsion system can be defined as:

$$\eta_p = \frac{\mathbf{P}_T}{\mathbf{P}} \quad (2.8)$$

where \mathbf{P}_T is the jet power and \mathbf{P} is the input power. The jet power is defined as:

$$\mathbf{P}_T = \frac{1}{2} \dot{m} c^2 = \frac{F^2}{2\dot{m}} \quad (2.9)$$

while, the input power is that of the applied potential difference, i.e.:

$$\mathbf{P} = VI. \quad (2.10)$$

By substituting equations 2.9 and 2.10 into equation 2.8, the following expression is obtained:

$$\eta_p = \frac{F^2}{2\dot{m}IV}. \quad (2.11)$$

The experimental setup used in this thesis in order to characterize the emission beam composition is what is known as a Time of Flight mass spectroscopy (ToF). See section 3 for description of the instrument. Given that the measurements taken by this apparatus are continuously through time, the summations can be rewritten as integrals of time. Starting by rewriting equations 2.7 and 2.4. If we define $I'(t) = I_{tot} - I_s$. To do so, one must first think back to the definition of mass flow rate:

$$\dot{m} = \int_0^{\dot{m}_0} d\dot{m} = \int_0^{I_{tot}} \frac{dI'}{\frac{q}{m}(t)} \quad (2.12)$$

but since $I'(t)$ decreases with time, it is most convenient to rewrite it as:

$$\dot{m} = - \int_{I_{tot}}^0 \frac{dI'}{\frac{q}{m}(t)} \quad (2.13)$$

Now, thinking back to the energy balance and the definition of a instantaneous specific charge, it is known that:

$$\frac{q}{m}(t) = \frac{1}{2V} \left(\frac{L}{t} \right)^2 \quad (2.14)$$

Substituting this to the previous equation, the mass flow rate is rewritten as:

$$\dot{m} = - \int_{I_{tot}}^0 \frac{2V}{L^2} t^2 dI' = - \frac{2V}{L^2} \int_{I_{tot}}^0 t^2 dI' \quad (2.15)$$

By integrating by parts:

$$\dot{m} = - \frac{2V}{L^2} \left[I' t^2 \Big|_0^\infty - 2 \int_0^\infty t I'(t) dt \right] \quad (2.16)$$

leading to the final form as:

$$\dot{m} = \frac{4V}{L^2} \int_0^\infty I'(t)tdt. \quad (2.17)$$

Similarly for 2.7, it is know that

$$F = \int_0^{m_0} c(t)d\dot{m} \quad (2.18)$$

from 2.3

$$F = \int_0^{m_0} c(t)d\dot{m} = - \int_{I_{tot}}^0 \sqrt{2\frac{2}{m}(t)V} \frac{dI'}{\frac{a}{m}(t)} \quad (2.19)$$

By substituting the equation 2.14 and simplifying, one gets:

$$F = -\frac{2V}{L} \int_{I_{tot}}^0 tdI' \quad (2.20)$$

Now by integrating by parts:

$$F = -\frac{2V}{L} \left[I't \Big|_0^\infty - \int_0^\infty I'(t)dt \right] \quad (2.21)$$

Leading to the final expression of thrust to be:

$$F = \int_0^\infty \frac{2V}{L} I'(t)dt. \quad (2.22)$$

Now, by substituting equations 2.22 and 2.17 into the efficiency equation 2.11, the result is:

$$\eta_p = \frac{\left[\int_0^\infty \frac{2V}{L} I'tdt \right]^2}{2IV \int_0^\infty \frac{4V}{L^2} I't^2dt}, \quad (2.23)$$

which can be further simplified to:

$$\eta_p = \frac{\left[\int_0^\infty I'(t)dt \right]^2}{2I_{tot} \int_0^\infty I'(t)tdt} \quad (2.24)$$

where I_{tot} is the total emitted current measured the the retarding potential analyzer (RPA).[6]

Chapter 3

Experimental Methods

This thesis consists on the study of several key properties of ionic liquids that have direct correlation with their efficiency as propellants in electrospray thrusters. Physical properties such as surface tension and conductivity are what facilitate the creation of the meniscus and thus the ion emission. The mixtures that shall be discussed are based on existing ionic liquids that have been previously used as propellants in electrosprays, as well as salts that contain ions of interest.

3.1 Single Tip Manufacturing

For the purpose of this thesis, it was crucial to have sharp single emitter tips as our ion source. This was due to the need to characterize the ionic liquids in a controlled and repeatable setup. In previous work done by Ph.D. Catherine Miller, it was seen that using full thrusters had too much variability.[16] These single emitters had several constraints, not only on the size, shape and material, but also on the mount design. The material selected for the tips was Carbon Xerogel, that is manufactured in-house. This is a very uniformly-porous material that has been developed and tested for the electrospray emitters in the past.[17] The main attractive quality for the research presented, is that it is a simple material to machine and work with. The shape restrictions placed on our tips were both experiment restrictions, but also for size restrictions placed by collaborators, who will use similar sources for different set of

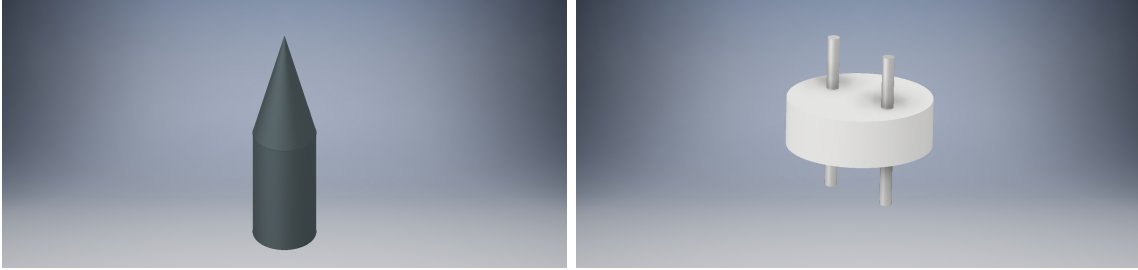
experiments.

The most important restriction placed on the tip was the maximum radius of curvature, which had to be $10\ \mu\text{m}$ with a cone angle of 30° . This restriction on the tip radius of curvature, comes from the strength of the electric field, and therefore the voltage, necessary in order to start emitting ions from the source. In other words, the sharper the tip, the lower the voltage that needs to be applied. Given that the testing of these tips was to be done in a very delicate experimental setup, the start up voltage had to be well below the arcing voltage of our spherical RPA. Moreover, sharp tips also help localizing the liquid meniscus better to prevent off-axis emission.

On the other hand, to meet third-party requirements, the single emitter should not be more than $9\ \text{mm}$ from the top of the base of the mount. Furthermore, the tips and their mounts had to be compatible with the geometry of a specific setup. This led to designing the single emitter setup in 4 parts: the tips, the mount that hold the tips in a centered and upright position, the ceramic material that would allow for the heating of the liquid uniformly, which was a restriction placed by our experimental interests and lastly, the base of the mount that connects everything to the vacuum chamber.

The tips were filed down using a small lathe and 3 different types of sanding-paper. For future works, it is suggested that in order to get a better tip, the final cut at the tip be made using a laser.[14] On average, the tips were $8\ \text{mm}$ tall to allow for some height adjustments without decreasing the overall volume of the single-emitter (See figure 3-1a).

The part shown in figure 3-1b was with which the tips were to be connected to both the power supply and the heat source. A mount made out of stainless steel was made in order to hold the tip in place. Stainless steel was selected for its conducting properties and its vacuum readiness. The design of this mount was such that the way the tip was held in place was through friction forces between the tip, the microfiber paper and the holder itself (See figure 3-2a). The reasoning between the use of the microfiber was to avoid having direct contact between the tip and the rest of the mount. It has been previously identified that if there is direct contact between the



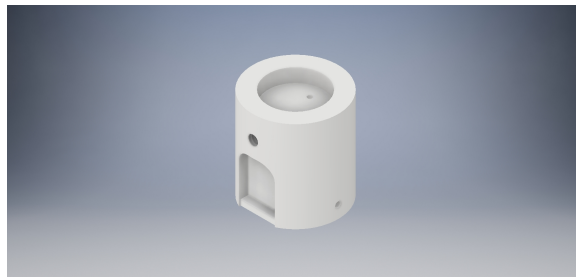
(a) Diagram exemplifying the ideal tip geometry of the Carbon Xerogel. (b) Diagram of the connector piece given by the sponsors.

Figure 3-1: First two out of the five components that composed the single emitter tip setup designed for this thesis.

tip and the holder, the erosion effects on the tip after firing are more severe.[3] Since the microfiber paper absorbs the ionic liquid, the liquid acts as the only connection between the tip and the body and decreases the electron removal from the tip.



(a) Diagram of stainless steel holder which held the tip in place while connecting it to the pins and the rest of the mount. (b) Diagram of PEEK mount used to attach the rest of the setup to the vacuum chamber.



(c) Diagram of ceramic body used to warm up uniformly the ionic liquid.

Figure 3-2: Components to the single emitter tip setup.

The ceramic body was made with a highly thermally conducting ceramic, Boron Nitride, that would facilitate an even warming of the liquids. Part of the liquid characterization is to find the relationship between temperature and conductivity.

Being able to warm up the liquids would allow us to add one more parameter to our matrix of results. This was done by placing a heater against the ceramic, while having a thermocouple on the opposite side to more accurately measure the temperature at which the body was at. Additionally, it also served as an insulator to avoid electronic connections between the tip and the vacuum chamber. The ceramic body had two side holes to allow the pins to be connected to the high voltage source via a screw (see figure3-2c).

Lastly, the base which held the rest to the mount onto the vacuum chamber was made out of PEEK (see figure3-2b). This material was selected because it has a very high melting temperature, which was necessary to hold our heater in place, at the same time that it is also vacuum safe.

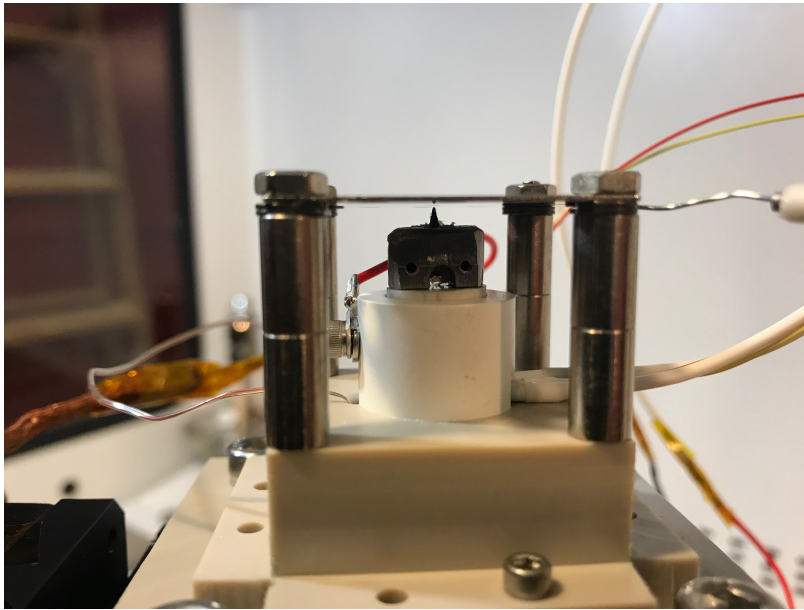


Figure 3-3: Picture of the complete single emitter tip setup mounted on the the vacuum chamber with the necessary connections.

3.2 Surface Tension Experiments

The surface tension experiments consisted of two parts: the measurement of the contact angle (θ) and the measurement of the height of the liquid column inside a capillary tube (h). These two values were necessary to extract the surface tension

value (γ) given by the capillary action equation

$$\gamma = \frac{\rho g D h}{4 \cos \theta} \quad (3.1)$$

where ρ is the density of the liquid, g the gravity's acceleration and D the diameter of the capillary tube.

3.2.1 Setup

The measurement of the contact angle was done by placing a drop of ionic liquid on a clean glass slide, same material as the capillary tube, and taking a side view picture. This picture was then uploaded into the computer and using an image processing software, ImageJ, the contact angle was extracted. (see figure 3-4). An additional step was done in order to account for the parallax error. This was done by modifying the image to remove the angle at which the picture was taken.

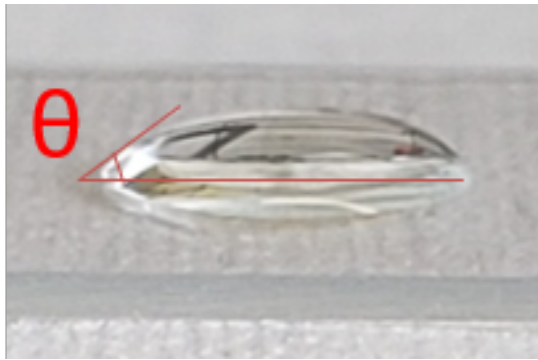


Figure 3-4: Example of a liquid drop on clean microscope slide.

The height of the column was measured in a similar way. The ionic liquid was placed in a small beaker and then a capillary tube of known inner diameter 1 mm, was held steady. The side view picture was then analysed using the same image processor as previously mentioned. (see figure 3-5)

Both the slides and the capillary tube were cleaned using an oxygen plasma to remove possible organic contaminants from their surface.

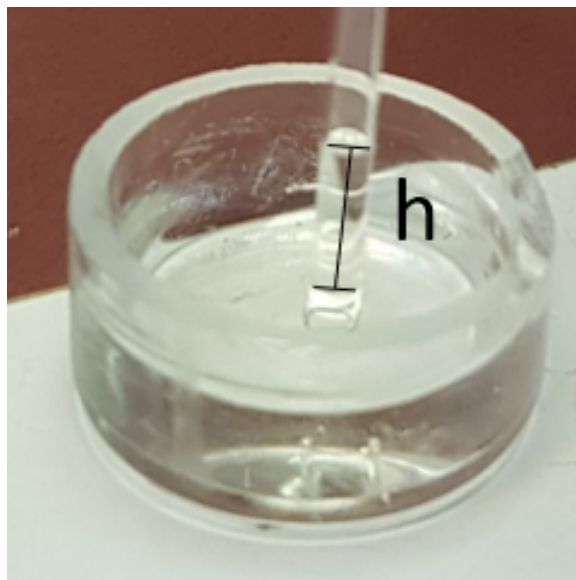


Figure 3-5: Example of a liquid column up a capillary tube.

3.3 Temperature vs. Conductivity

The temperature versus conductivity measurements were the backbone of this thesis. The aim of these experiments was to determine the a salt to ionic liquid weight percentage ratio, as well as the best temperature at which to fire the mixtures, that matches with the desired properties. The need to understand the correlation between the conductivity of these specific mixtures and their temperature, led to the extensive investigation done in this thesis.

3.3.1 Setup

The experimental setup (see figure 3-6) consisted of a conductivity-meter to measure both the conductivity and the temperature. The temperature control came from a hotplate in which an aluminium cylinder that surrounded the glass vial with the mixture, was placed. This cylinder served as a thermal conductor to help warm up the mixture faster. Around this cylinder, a small drybox was placed. This drybox helped remove the humidity of the environment by flowing nitrogen into the system. Most of the salts and the ionic liquids that were used to make the mixtures were extremely hydrophilic and if left out, a noticeable difference in conductivity measurements could



Figure 3-6: Picture of the heating setup. On the left there is the heating plate, the dry box connected to the nitrogen and the conductivity meter probe. On the right, is the conductivity meter.

be seen.

3.4 Retarding Potential Analyzer Experiments

The Retarding Potential Analyzer (RPA) was one of the key instruments used to characterize the emission beam. RPAs allow for the measuring of the energy distribution of the ionic beam. This is done by applying a voltage, V_{st} , that "stops" the incoming ions, of charge "q", with equal or less kinetic energy than that given by equation 3.2, from reaching the current collector. This allows us to characterize the current as a function of the voltage.

$$qV_{st} = K_{RPA} \quad (3.2)$$

The ionic beam is composed of cluster of ions, normally found as dimer or trimers, that may experience fragmentation in two main regions: the acceleration region and the field-free region. The acceleration region is that between the tip and the extractor grid, while the field-free region is the rest of the ion's trajectory once it has

passed the extractor grid. In the field-free region, there is no external force adding to the kinetic energy of the ions. Therefore, fragmentation of the clusters causes the new kinetic energy of the broken ions to be calculated with the equation:

$$\frac{K_{bi,FFst}}{qV_0} = \frac{m_{bi}}{m_{pi}} \quad (3.3)$$

where q is the ion charge, V_0 is the source potential, m_{bi} is the mass of the broken ion and m_{pi} is the mass of the parent ion. This causes the current versus voltage curve to have multiple steps. (see figure 3-7)

However, when fragmentation occurs within the acceleration region, given that the electric field is present, the broken ions can drastically change their kinetic energy. Lighter ions, such as monomers, reach higher velocities, making it possible to neglect their initial velocities and thus, be described with equation 3.4 :

$$K_{bi,st} = qV_0 \left(\frac{m_{bi}}{m_{pi}} + \frac{V_{br}}{V_0} \left(1 - \frac{m_{bi}}{m_{pi}} \right) \right) \quad (3.4)$$

where V_{br} is a function of the position at which the fragmentation occurred. This spatial dependency is what causes the current vs. voltage curves to have a slope in between fragmentation steps, (see figure 3-7b).[16]

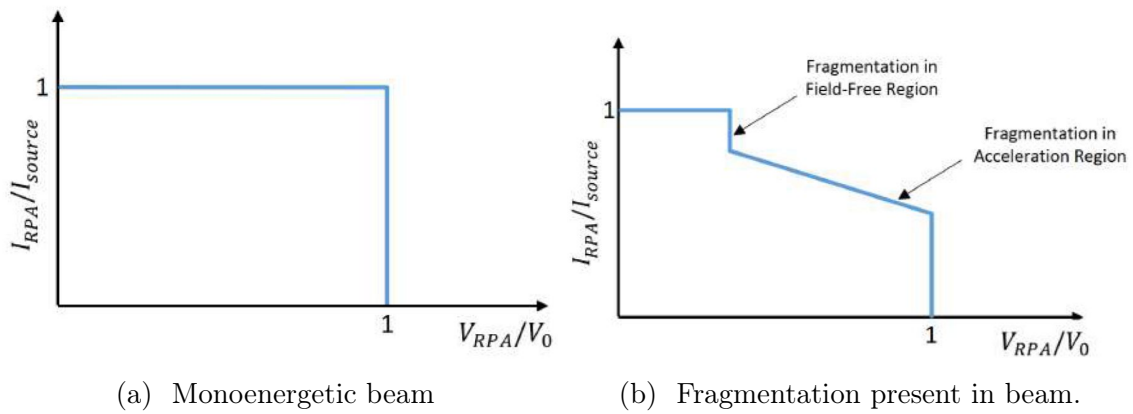


Figure 3-7: Idealized RPA curves.[16]

3.4.1 Setup

The experiments in this thesis were done using a spherical RPA. The spherical RPA was designed and built by a Ph.D student from SPL, Catherine Miller.[16] The idea behind using a large spherical RPA is to capture most, if not all of the ionic beam to make sure to detect the composition of the beam seeing as it might not have a uniform profile, as is normally by small planar RPAs. This RPA is composed of four grids. The first grid, or that closest to our ILIS, is grounded to make ensure a field-free region between the extractor and the RPA. The second grid sets the retarding voltage of the RPA which slows down the incoming ions. The third grid is always set at -30V and serves as a electron repelling grid. This grid prevents secondary electrons from leaving the collector plate and artificially changing the magnitude of the measured currents. (see figure 3-8)

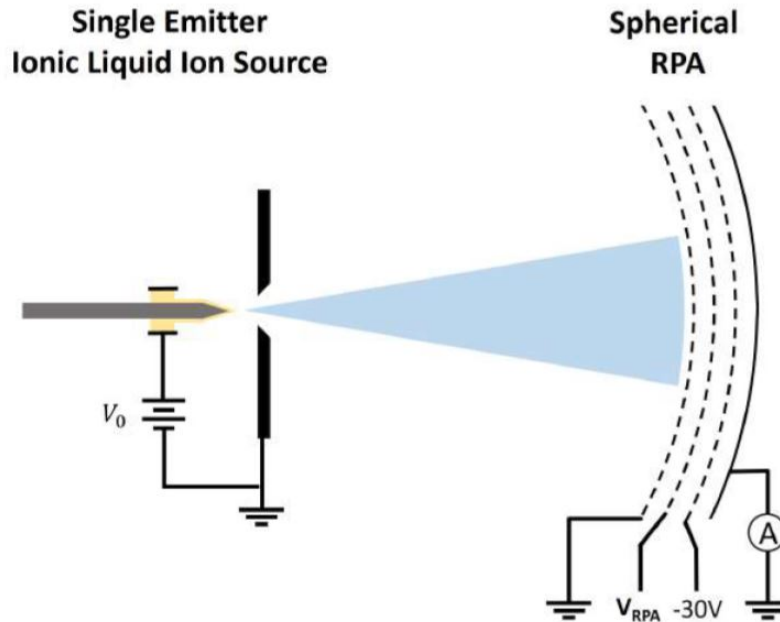


Figure 3-8: Picture of the spherical RPA setup designed by Catherine Miller. [16]

3.5 Time of Flight Mass Spectrometry Experiments

Similarly to the RPA, the Time of Flight system used in this thesis was designed by Catherine Miller.[16] The Time of Flight mass spectrometer (ToF), as the name suggest allows for mass distribution measurements of an ion beam. This is done by having a known length section, inside or as part of the vacuum chamber, known as the "flight region". In order to calculate the speed at which the ions are moving, the exact time of entry to this section is controlled by a shutter or deflector, and the final time is recorded with the collector plate at the end that measures the current at a given time. The flight time of a single ion can be calculated using:

$$t_f = L\sqrt{\frac{m_i}{2qV_0}} \quad (3.5)$$

where "L" is the length of the flight region. However, as was mentioned in the RPA section, the fragmentation of the cluster of ions exists in 2 different regions and in both cases, however the flight time of the ions that fragmented in the field-free region does not change. Fragmentation in the acceleration region is seen in the ToF measurements, in the slopes in between the steps. Taking the energy of the broken ion in the acceleration region given by equation 3.4, the flight time of the broken ion can be extracted as:

$$t_{bi} = \frac{L}{\sqrt{\frac{2qV_0}{m_{pi}} \left(1 + \frac{V_{br}}{V_0} \left(\frac{m_{pi}}{m_{bi}}\right)\right)}} \quad (3.6)$$

The flight time of the parent ion, on the other hand, could be calculated using the ratio:

$$\frac{t_{bi}}{t_{pi}} = 1 + \frac{V_{br}}{V_0} \left(\frac{m_{pi}}{m_{bi}} - 1\right) \quad (3.7)$$

This is important because it allows for the distinguishing between single molecules that where single from the beginning and those that broke down at a later stage. This difference can be seen in figure 3-9b. The height of this slope indicates the number of dimers that break down in the acceleration region. Meanwhile, in a monoenergetic beam (figure 3-9a) the height of the steps indicates the number of dimers or monomers.

On the other hand, in the field-free region the flight time of the broken ion is described by:

$$t_{bi} = L\sqrt{\frac{m_{pi}}{2qV_0}} \quad (3.8)$$

This implies that it is not possible to distinguish between the dimers present in a monoenergetic beam and dimers that broke in the field free region.

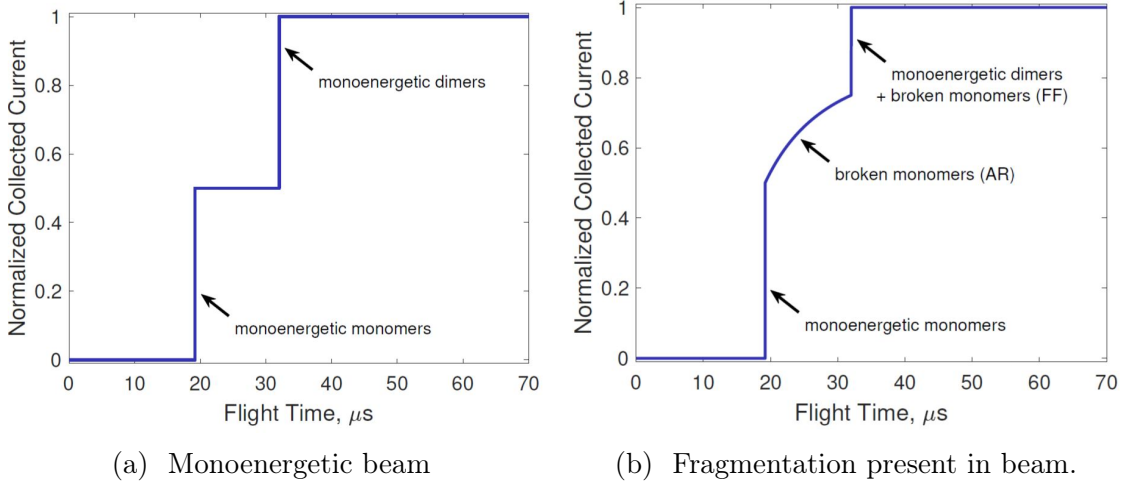


Figure 3-9: Idealized ToF curves.[16]

3.5.1 Setup

As previously stated, the experiments in this thesis were done using the experimental setup built by Ph.D Catherine Miller. The ToF system consisted of a deflection gate and a channeltron electron multiplier with which acted as the detector. The deflection gate allowed the control of the initial time of entry of the ions. Furthermore, we could use it to pulse the beam at a known and controlled frequency in order to make several measurements and average the results.[16]

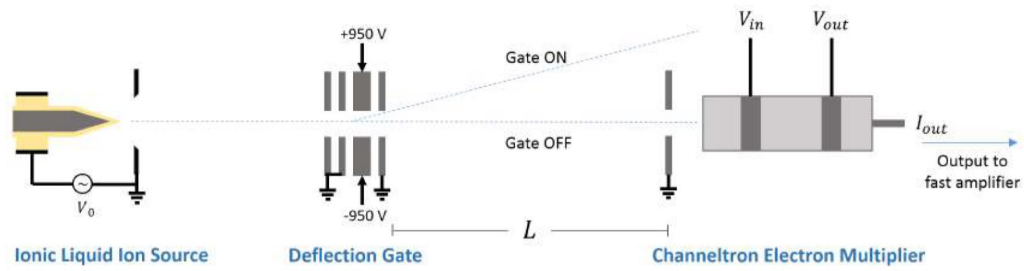


Figure 3-10: Picture of the ToF setup designed by Catherine Miller. [16]

Chapter 4

Molecular Dynamics Simulations

In this thesis, molecular dynamics simulations (MDS) are explored in order to further understand the ionic emission from a mixture and how it is different than that from a pure ionic liquid. The use of MDS for mixtures is a relatively new approach to predict their performance as ionic sources. The simulation code used, was written by PhD candidate Thomas Coles. The simulations were run in a cluster with infiniband network and AMD K10 processors, arranged in nodes with 8 or 12 cores.[4]The visualization of the simulations was done using "Visual Molecular Dynamics".[9, 15]

4.1 Theory

In molecular dynamics, the forces experienced by a single charged molecule are modeled as force fields and each atom is assigned a partial charge. As most of the force fields used for ionic liquid simulations, the code is based on OPLS-AA, originally designed for general molecules. The intra-molecular forces use Lennard-Jones approximations to model the Coulomb and Van der Waals forces to maintain their structure. The simulations uses Large-Scale Atomic/Molecular Massively Parallel Simulator (LAMMPS), an open source code distributed by Sandia National Laboratories.[18, 10, 4]

4.2 Selected Properties.

The MDS were done by creating a droplet of approximately 15 nm in diameter. This size of droplet does not allow for the creation of a Taylor Cone and therefore, the electric field that is applied to the simulation, has to be that which can be expected for the IL to experience at the emitter tip. The first step to designing this droplet was creating a grid with the number of desired ion pairs. This is then collapsed to the droplet shape by a radial inward force, allowing for "excess ions" to be removed. Then the temperature is set to 300K, room temperature, while removing the strong potential field and allowing for the coalescence force to preserv the shape of the droplet.[22]

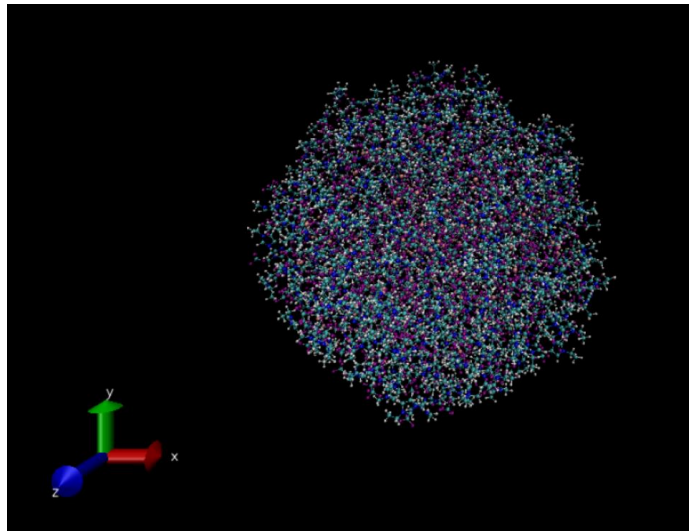


Figure 4-1: Example of a $EMIBF_4 + 27wt\%LiBF_4$ 15nm droplet with 720 neutral pairs.

The electric fields that the ions can expect to experience at the liquid/vacuum interface, both in a thruster and the experiments described in this thesis are roughly of the $10^6 V/m$ order of magnitude. This is the field that leads to the instability that forms a sharp meniscus, i.e. the Taylor cone. However, a field strength of approximately $0.1 V/\text{\AA}$ can be expected very close to the tip making this a good bench mark for the electric field selected in the simulations. However, the geometry of the electric field applied to the MDS, was not the same of that applied in the

experiments. The MDS electric field was a uniform field similar to the one that can be expected between two parallel infinite plates along the x-axis. Additionally, given the symmetry and size of the droplet, it is possible to simultaneously observe what is happening on both the positive and the negative mode. The conditions selected for the simulations on these thesis were based on similar simulation work done by Ph.D Tom Coles [4] and Benjamin D.Prince et al. [19]

As previously mentioned, this thesis' main focus is on the mixtures of $EMIBF_4$ and $LiBF_4$. Given time restrictions, only the pure ionic liquid and two mixtures, at 27wt% and 15% were simulated. The ToF experiments were taken at startup voltages of 1.87 kV for pure $EMIBF_4$ and 1.89 kV for the 27wt% mixture. Therefore, these conditions were also simulated, along with another standardized voltage that allowed for the comparison amongst three different concentrations. See table 5.7.

Mixture Simulated	E Field (V/Å)	# of Pairs	Sim. Time (ps)
$EMIBF_4$	7.00	240	10.00
	2.00	240	10.00
$EMIB_4 + 27wt\%LiBF_4$	7.00	240	10.00
	2.00	240	20.00
		720	9.937

Table 4.1: Matrix of the properties selected for the different simulations run. The second column are the values of the electric field applied to the simulation. These were all along the x-axis. The third column are the number of total neutral pairs that make up the initial droplet. Lastly, the fourth column is the total real time that has been simulated. All runs were done at a constant temperature of 300 K.

Chapter 5

Results and Discussion

In this chapter, both experimental and simulation results are presented. Given the time limitation, it was fortunate that there was data available for one concentration, apart from the pure ionic liquid that was used as the solvent. It is important to note that these results have laid the foundation in order to accomplish the original goals of this thesis in future works. The biggest time sink came from the single tip emitter production process and the tight tolerance set on the tip curvature radius.

5.1 Surface Tension Results

The results of these experiments are shown in figure 5-1. As was previously mentioned in chapter 3, the data analysis was done using an image processing program called "Image J". The error margins are the equivalent error obtained by counting the range of pixels at which both the angle and the height could be in. This graph indicates that as one increases the weight percentage of the salts, the surface tension starts to decrease. The surface tension of a liquid has been found to have a correlation with the emitted current following the equation in the case of pure ionic emission:

$$I = \frac{32\pi\gamma^2 K}{f(E, \epsilon)} \quad (5.1)$$

where γ is the surface tension, K the conductivity.[5] Thus, the graph would initially suggest that the goal should be to use lower concentration of salt since the current appears to be highly sensitive to the surface tension. Yet, once the first $5wt\%$ is added to the mixture, the further increase in weight percentage, no longer has such a drastic effect on the surface tension. Adding higher concentrations of salt causes it to act as a surfactant.

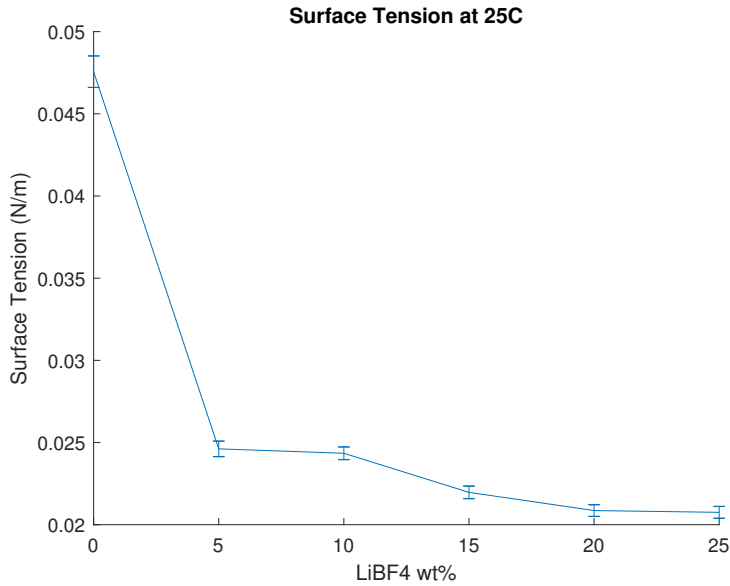


Figure 5-1: Surface Tension vs the salt weight percentage in the mixture at a constant $25^{\circ}C$.

The main limitation to these results was the quality of the images. Moreover, it is important to keep in mind that the assumption that the glass of the slides and the capillary tube were the same, was made.

5.2 Temperature vs. Conductivity Results

The results of these experiments can be found in figures 5-2 and 5-3. The error bars indicate the precision of the conductivity meter. To see all the individual plots, refer to appendixes A and B. It is important to note that higher concentrations of salt were studied, but a mixture saturation point was identified right after $30 wt\%$ making them not useful for the goal application of this thesis. From the obtained results,

there are several trends that stand out. Firstly, in figure 5-2, at all concentrations we see that there is a proportionality between temperature and conductivity. This means that the higher the temperature, the higher the conductivity. This points to a desired operating/testing temperature that would be limited only by our heating capabilities. Secondly, the strength of the effects temperature has on the conductivity seem to decrease as the $wt\%$ increases.

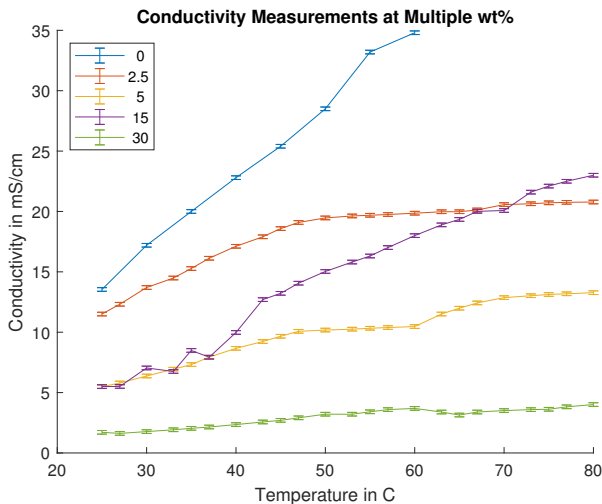


Figure 5-2: Conductivity vs Temperature in C at constant $LiBF_4$ wt%.

On the other hand, there is figure 5-3. In this graph, it is possible to see that there is no simple relationship between the conductivity and the mixture concentration. The first and most obvious observation is that the highest conductivity is reached when there is no salt added to the ionic liquid, i.e. $0wt\%$. Secondly, there seems to be an inversely proportional trend between the two properties, which leads to the hypothesis, the higher the concentration, the lower the current. Nonetheless, this is not true for the local maximum at $15wt\%$, making this the most interesting concentrations for further testing.

In the midst of testing, a curious colour change occurred as a consequence of the heating experiments. This led to a series of side experiments in hopes to determine the reason for this colour change. Examples of the tracking of this colour change can be found in appendix C. In summary, it is believed that this is a consequence of the Li^+ ions reacting with the $[EMI]^+$ ions when heated. This theory comes from

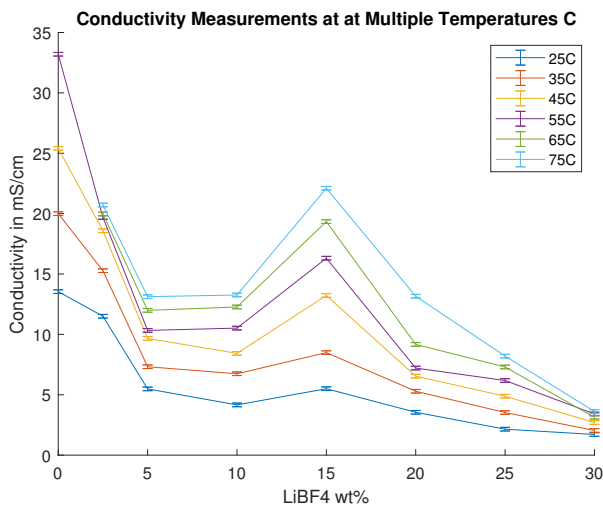


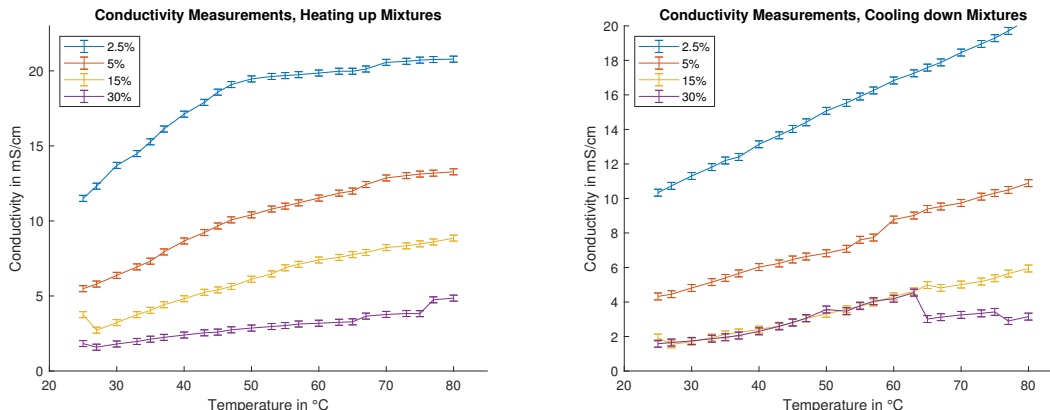
Figure 5-3: Conductivity vs $LiBF_4$ wt% at constant Temperatures in C.

the fact that any concentration of salt that is greater than zero, i.e. is a mixture, is heated past $30^{\circ}C$ there is a change in colour. The ionic liquid was heated but no colour change was seen. The higher the salt concentration the stronger the colour change. Moreover, the higher the temperature the mixture is heated to, the darker the colour change. Lastly, it is important to note that the colour does not return to normal after long observation periods. All these experiments were done in the small drybox with nitrogen flowing through and warmed up to the same temperatures using the same heating profile and technique. These experiments were even done without the conductivity meter probe to ensure that this was not a reaction with the silver plates used for the measurements. Nevertheless, more experimentation is required in order to back up this hypothesis.

Another interesting trend that was studied was what other effects heating the liquid multiple times had. This was inspired by the change in colour. It was important to investigate whether this change in colour was the only lasting effect heat was having on the mixture, or if it was in fact changing the conductive properties. This was done by selecting a handful of the concentrations and taking measurements both ramping up and down the temperatures as is shown in figure 5-4.

What is seen from these results, is the conductivity changes at the same temperature depending on whether the temperature is being increased or decreased. Higher

conductivities are reached on the warm up, than on the cool down. The cool down does not seem to match the warm up initial and final conductivities, which because more evident at higher $wt\%$. Furthermore, the path that are followed in the ramp up and the ramp down are not the same. This might be a consequence of the speed at which things were being warmed up or cooled down, thus, more extensive testing is recommended.



(a) Conductivity vs Temperature in C at constant $LiBF_4 wt\%$ during the heat-up process. (b) Conductivity vs Temperature in C at constant $LiBF_4 wt\%$ during the cool-down process

Figure 5-4: Comparison of heat-up and cool-down conductivity vs. temperature curves for multiple mixtures.

When comparing multiple warm up runs, there is no clear pattern suggesting that there is a change to how the conductivity responds to temperature after being to expose to higher temperatures previously. For more detailed graphs see appendix C. Moreover, ramp up and down experiments would be further necessary to settle the effect temperature variations has over liquid properties as a function of time.

5.3 Time of Flight Results

In this section, the measurements used were produced by Ph.D Catherine Miller. They were shared directly through personal communication to the author of this thesis. However, all the analysis of results was done by the author of this thesis. It is important to keep in mind that these ToF measurements were only done for the

positive mode of the liquids.

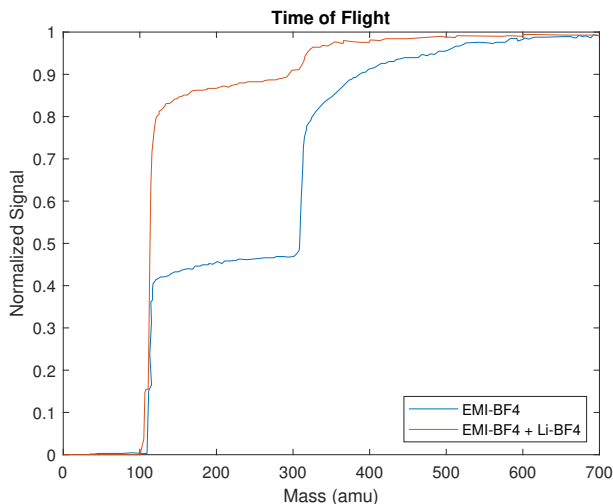


Figure 5-5: Normalized current vs mass, ToF graph produced by Catherine Miller, for both the pure $EMIBF_4$ ionic liquid (blue curve) and the mixture of this same liquid with 27wt% of $LiBF_4$ salt (red curve).

When looking at the curves on figure 5-5, the first thing that one notices are the multiple steps present in both curves. As was previously mentioned in chapter 2, the steps are a consequence of emission of ion-clusters of different masses. As was expected from the results found in previous works, pure ionic emission was not without efficiency loss. This can be seen at the very top of the pure ionic liquid curve, where the step is rounded given the emissions of heavily solvated ion fragments. This emission characteristic is not as present in the mixture emission. However, it is still possible to see the monomer and dimer steps, which contribute more strongly to the inefficiency. Furthermore, the two large steps on the pure $EMIBF_4$ cure indicate the emission of EMI^+ monomers, which is the first step starting from the left, and $EMI^+(EMIBF_4)$ dimers. This is determined by the mass at which the step begins.

In a similar fashion, the 27wt% $LiBF_4$ mixture curve shows four different steps. Starting from the left, there are: $Li^+(LiBF_4)$ dimer, EMI^+ monomer, $Li^+(LiBF_4)(EMIBF_4)$ trimer and lastly $EMI^+(EMIBF_4)$ dimer. From figure 5-5, one can determine there were no Li^+ monomers. That aside, there is a significant decrease in the emission of heavily solvated ion fragments.

It is possible to determine the breakdown of the composition of the beam by the measuring the heights of the curves as is done in tables 5.1 and 5.2.

Type of Ion	Beam Composition %
EMI^+	43.93
$EMI^+(EMIBF_4)$	56.07

Table 5.1: Beam composition breakdown for the pure $EMIBF_4$ ionic liquid ToF. The values were obtained by measuring the heights of the different steps of the pure ionic liquid curve in figure 5-5

Type of Ion	Beam %
$Li^+(LiBF_4)$	14.68
EMI^+	70.87
$Li^+(LiBF_4)(EMIBF_4)$	2.57
$EMI^+(EMIBF_4)$	6.93

Table 5.2: Beam composition breakdown for the $EMIBF_4$ ionic liquid mixed with 27wt% of $LiBF_4$ ToF measurements. The values were obtained by measuring the heights of the different steps of the curve of the 27wt% of $LiBF_4$ mixture, figure 5-5

From these tables, we see that although there are more species of ions in the case of the salt mixture, we do see that that the monomer EMI^+ is a greater percentage of the the beam than what is seen in the pure $EMIBF_4$ curve.

Moreover, using equation 2.24 and applying it to figure 5-5, the following efficiency values are obtained:

Ionic Liquid	η_p
$EMIBF_4$	0.9268
$EMIBF_4 + 27wt\%LiBF_4$	0.9468

Table 5.3: Efficiency values for the pure ionic liquid $EMIBF_4$ and the mixture of this same liquid with 27wt% of $LiBF_4$ salt. These values were extracted from the ToF graph (figure 5-5).

This tells us that there is a slight increase in efficiency of the liquid by the inclusion of the salt. Yet, it is important to compare our results with a two species approximation to validate our results. To do so, one must first look back at equations 2.7 and 2.4 and by substituting them in 2.11, the efficiency for only 2 species, can be calculated using:

$$\eta_{2s} = \frac{\left(\dot{N}_1\sqrt{m_1q_1} + \dot{N}_2\sqrt{m_2q_2}\right)^2}{\left(\dot{N}_1q_1 + \dot{N}_2q_2\right)\left(\dot{N}_1m_1 + \dot{N}_2m_2\right)} \quad (5.2)$$

which, if $I_1 = \dot{N}_1q_1$ and $I_2 = \dot{N}_2q_2$ are the currents produced by those species and by defining $f_1 = \frac{I_1}{I_T}$ and $f_2 = \frac{I_2}{I_T}$, it can be rewritten as the following:

$$\eta_{2s} = \frac{\left(f_1\sqrt{m_1} + f_2\sqrt{m_2}\right)^2}{\left(f_1m_1 + f_2m_2\right)}. \quad (5.3)$$

For the two cases discussed on this thesis, the 2 species that were selected were the ones that had the highest percentages and significantly different masses in table 5.1 for the pure $EMIBF_4$ case and table 5.2 for the 27wt% mixture. The masses that were very similar were combined into one. For each one of these species, their beam percentage and mass are in table 5.4.

Mixture	Charged Molecule	Beam %	Mass (g/mol)
$EMIBF_4$	EMI^+	48.77	111.0
	$EMI^+(EMIBF_4)$	51.23	308.8
$EMIB_4 + 27wt\%LiBF_4$	$EMI^+ + Li^+(LiBF_4)$	85.55	111.0
	$EMI^+(EMIBF_4) + Li^+(LiBF_4)(EMIBF_4)$	14.45	308.8

Table 5.4: Selected 2 species, beam composition percentage and mass of ions for the $EMIBF_4$ ionic liquid and for the 27wt% $LiBF_4$ mixture, taken from the ToF measurements (figure 5-5)

By substituting these values into the equation 5.3, the following values for the approximate efficiency were obtained:

Ionic Liquid	η_{2s}
$EMIBF_4$	0.9417
$EMIB_4 + 27wt\%LiBF_4$	0.9561

Table 5.5: Efficiency values for the pure ionic liquid $EMIBF_4$ and the mixture of this same liquid with 27wt% of $LiBF_4$ salt. These values were extracted from the ToF graph (figure 5-5) and using the 2 species approximation (see equation 5.3).

When comparing these values to those previously obtained in table 5.3, it is clear that the two species approximation has higher values in both cases. Nonetheless,

this is to be expected given that only having 2 types of species would decrease the polydispersive effect. That is why, it is to be expected that the values in table 5.5 are higher since they act as the upper limit. However, an important take away is that in both cases, the efficiency of the mixture is higher than that of the pure ionic liquid.

Likewise, the specific impulse of a propulsion system can be calculated with:

$$I_{sp} = \frac{F}{\dot{m}g} \quad (5.4)$$

and, given equations 2.22 and 2.17, its final form is:

$$I_{sp} = \frac{L \int_0^\infty I' dt}{2g \int_0^\infty I' t dt}. \quad (5.5)$$

With this equation, we can calculate what the reduction of the I_{sp} is when adding the solid salt and for the pure ionic liquid by defining it as:

$$R_{I_{sp}} = \frac{I_{sp}}{I_{sp_{monomer}}} \quad (5.6)$$

R_{ISP} Method	$EMIBF_4$	$EMIBF_4 + 27wt\%LiBF_4$
Integration	0.6160	0.8467
2 Species Approximation	0.7015	0.8719

Table 5.6: I_{sp} reduction calculated using both the 2 species approximation (see equation 5.3) and the integration method (see equation 2.24).

This last value is very helpful for determining how the emission of other species is affecting how much of the maximum specific impulse that would be possible to obtain if we only have single ion emissions. Lastly, if we compare the specific impulse of both liquids, by dividing the $R_{I_{sp}}$ from table 5.6, we realise that there is an increase in specific impulse of 27.25% by adding the salt.

Mixture Simulated	E Field ($V/\text{\AA}$)	Current (nA)	Beam Composition	
			Type of Ion	%
$EMIBF_4$	2.00	Not available	EMI^+	0
			$EMI^+(EMIBF_4)$	100
	7.00	94.27	EMI^+	83
			$EMI^+(EMIBF_4)$	17
$EMIBF_4 + 27wt\%LiBF_4$	2.00	40.40	EMI^+	100
	7.00	No Emission	EMI^+	0

Table 5.7: Results obtained from different simulation.

5.4 Simulations

There are multiple results that can be extracted from the results table of the simulations 5.7. From the pure ionic liquid, there was an increase in emitted current as the electric field applied increased. Likewise, the higher the applied field, the higher the percentage of the beam that was composed of EMI^+ ions. It was seen that the emitted current was lower for the mixture than for the pure ionic liquid when applying the same electric field since we did not see any emission in the simulated time. When applying a very high electric field to the droplet of the pure ionic liquid, it was possible to get a breakdown beam composition of 83% EMI^+ and 17% $EMI^+(EMIBF_4)$.

5.5 RPA Results

Unfortunately, there was only time to do but one RPA measurement for the pure ionic liquid $EMIBF_4$, figure 3-7. This measurement was taken using the tips and experimental setup described in section 3. In this graph, it is possible to see the current drops given the fragmentation of the different species. From left to right, the first tall drop is from dimers to monomers, the second step are trimers to dimers and last we have a final drop of the monoenergetic ions. These steps were the fragmentation of these ion clusters in the field free region. In between these steps, we have slopes that represent the fragmentation of the dimers in the acceleration region and then the second slope is the fragmentation of dimers, trimers and other big ion clusters in the acceleration region. Given the heights of the steps, compared to those of the

slopes, it can be determined that most fragmentation occurs in the field free region, which means that the beam is not going to be as energetic given that most of the ions that are being accelerated are heavier than a single ion and they will not lose their "extra weight" in time to reach higher speeds. Nevertheless, this is not necessarily bad given that if they did fragment, it would increase the polidispersity in the beam.

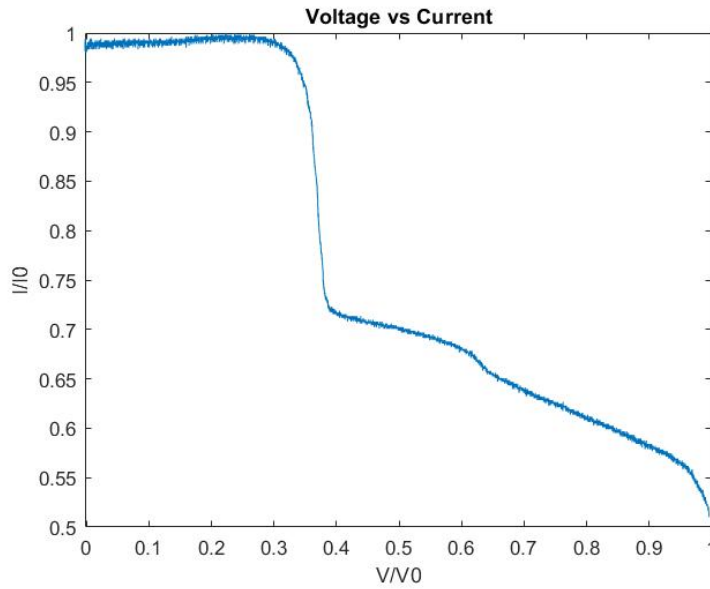


Figure 5-6: Normalized Current vs Normalized Voltage for pure $EMIBF_4$ ionic liquid.

Chapter 6

Conclusion and Future Work

In this chapter, the conclusions that can be drawn from the results section shall be discussed as well as what these results might imply about the use of these mixtures as ionic sources for electrospray propulsion. It goes without saying that there are always more questions to be answered and therefore future work and paths will also be proposed throughout the chapter.

6.1 Conclusions

From the results described in chapter 4, there are multiple conclusions that can be reached. Firstly, surface tension, in the range that was tested, experienced a sharp drop when the salt was first added to the ionic liquid. However, it seemed to start plateauing quickly at higher concentration of salt in the mixture. This leads to the belief that the decrease on surface tension is not drastic enough to discard choosing higher concentrations as viable options.

Secondly, in a purely qualitative manner, it is possible to conclude from observations done in this thesis that the viscosity of the mixture increases along with the increase in concentration. From the literature review, we know this to be a negative trait of the liquids since viscosity has an inverse relationship with the conductivity of the liquid. This is something that was confirmed in the conductivity versus concentration graphs. While keeping the temperature constant, it was seen that for the

most part, the higher the concentration, the lower the conductivity. Nevertheless, that relationship proved to not be as simple since a local maximum was measured at 15wt%.

Thirdly, the trend found between the temperature and conductivity, at all concentrations of the mixture, point to the higher the temperature, the higher the conductivity will be. However, the higher the concentration of salt, the smaller the effect the temperature will have on the increase of the conductivity of the mixture. Additionally, there appears to be a "temperature limit" placed by the possibility of chemical properties changing. Further research into this topic is recommended.

Lastly, the addition of the salt into the ionic liquid, at 27wt% led to an increase in efficiency of 2.11%. This is mainly attributed to the large percentage of the emitted beam being a single EMI^+ ion. Furthermore there was an increase in specific impulse of approximately 27% making the additions of the salt a very attractive way of improving electrospray thruster specific impulse, especially given the simplicity of adding salt to a readily available ionic liquid. Furthermore, it is important to point out that 27wt% was not even the most promising candidate.

6.2 Experimental Future Work

Future experiments will be necessary to test out the theory of an optimal mixture concentration. Ideally, the full matrix of experiments would consist of not only firing all the concentrations and gathering both RPA and TOF data, but also, other mixtures would be investigated. Other suggested mixtures are 1-Butyl-3-Methylimidazolium Iodide (BMI-I) as the solvent and Lithium Iodide (Li-I) as the salt. When experimenting with another mixture, it would be important to see if the change of colour, indicative of possible chemical reactions, also occurs. Yet, to get further information on the colour change, analysis such as calorimetry or IR spectroscopy would be recommended.

By doing this liquid next, it would help determine if the change in colour was in fact a reaction the lithium molecules were having with the EMI molecules of our

current mixture.

For future experimentation, it is also recommended that the tip process includes the laser in the lab as part of the single emitter tip manufacturing. The tip manufacturing was by far the bottle neck of this thesis. The time it took to make a sufficiently sharp tip left for a lot of improvement. The recommend path forward is to keep the current process to shape the tip up to a tip radius of $50\mu m$, which can be quickly achieved in 2 hours, and then proceed to sharpen the tip to a radius of $10\mu m$ using the laser. It is believed that once the laser is re-calibrated and the pattern to sharpen the tip is done, we could sharpen each individual tip in 5 minutes.[14]

6.3 Simulations Future Work

The simulations that would be a great next step to this thesis are molecular dynamic simulations of the different mixtures. Ideally, we would be able to replicate the results obtained experimentally and as a result, find the explanation of why we saw those results. Furthermore, this would help speed up the process of selection of the optimal mixture concentration, without having to run all the matrix of experiments. Additionally, it would be interesting to extract the ion density distribution at the layers closest to surface in order to further explain why certain clusters and monomers are easier to extract than others. In other words, it would be possible to explain we do not see single Li^+ emission in our ToF measurements.

Appendix A

Individual Conductivity vs. wt% at constant Temperature Graphs

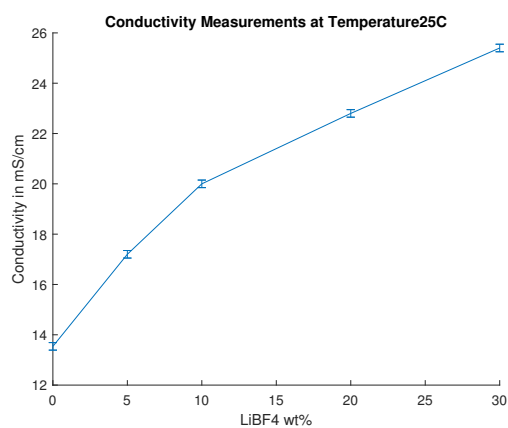


Figure A-1: Conductivity vs. wt% at a constant temperature of 25°C

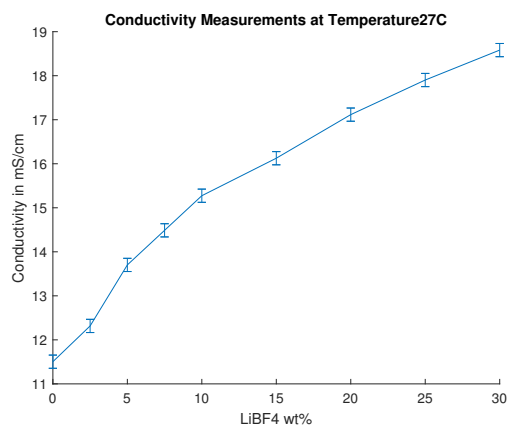


Figure A-2: Conductivity vs. wt% at a constant temperature of 27°C

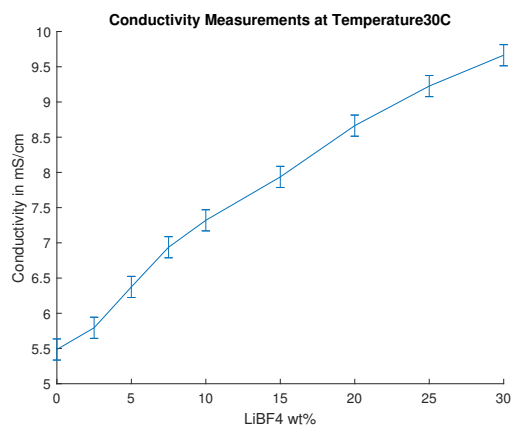


Figure A-3: Conductivity vs. wt% at a constant temperature of 30°C

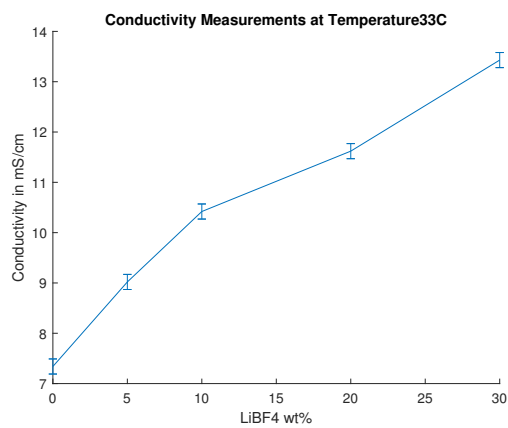


Figure A-4: Conductivity vs. wt% at a constant temperature of 33°C

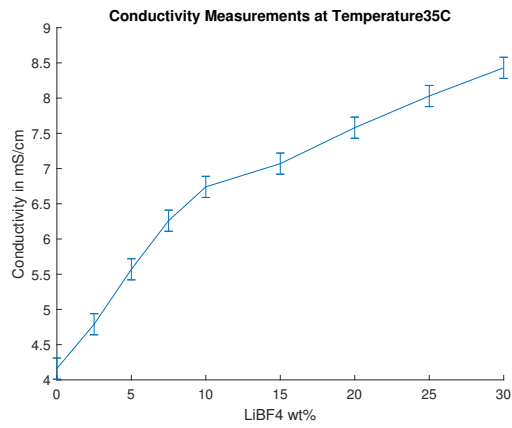


Figure A-5: Conductivity vs. wt% at a constant temperature of 35°C

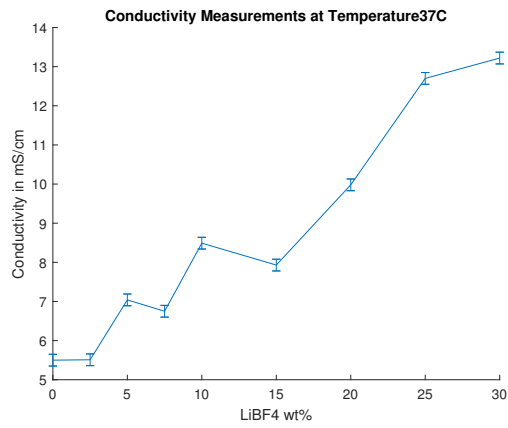


Figure A-6: Conductivity vs. wt% at a constant temperature of 37°C

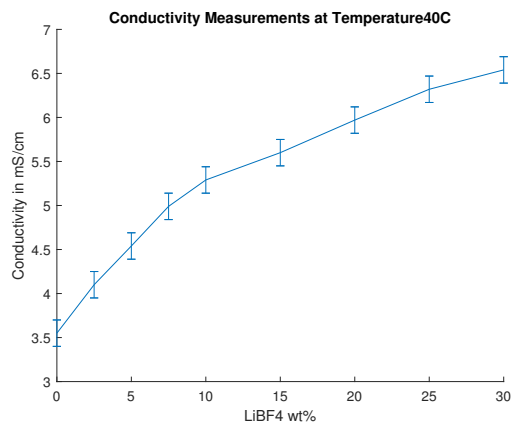


Figure A-7: Conductivity vs. wt% at a constant temperature of 40°C

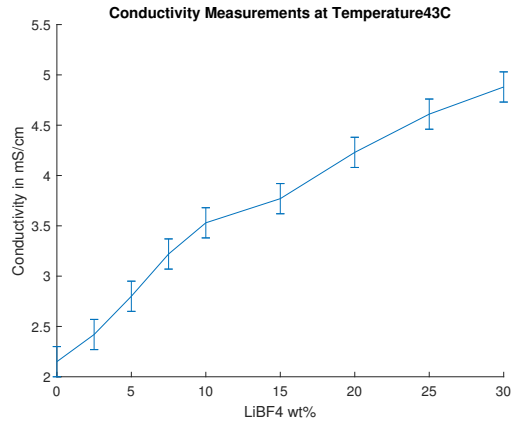


Figure A-8: Conductivity vs. wt% at a constant temperature of 43°C

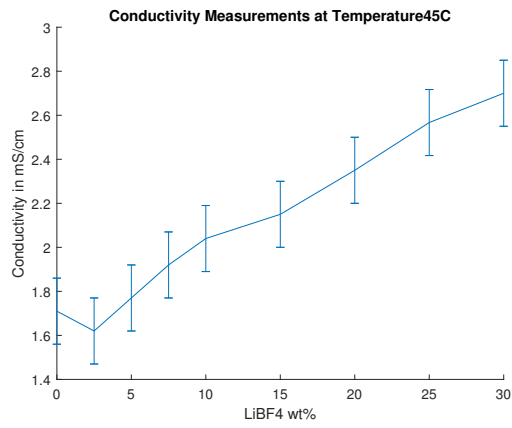


Figure A-9: Conductivity vs. wt% at a constant temperature of 45°C

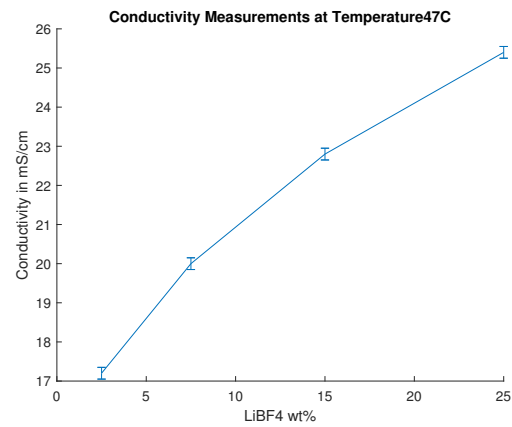


Figure A-10: Conductivity vs. wt% at a constant temperature of 47°C

Figure A-11: Conductivity vs. wt% at a constant temperature of 50°C

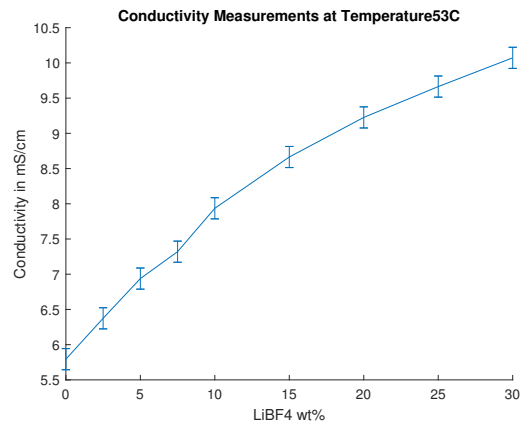


Figure A-12: Conductivity vs. wt% at a constant temperature of 53°C

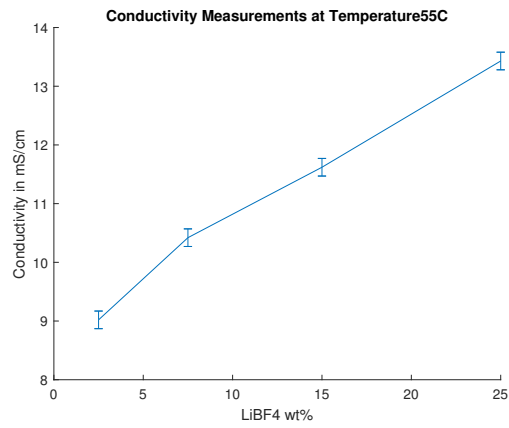


Figure A-13: Conductivity vs. wt% at a constant temperature of 55°C

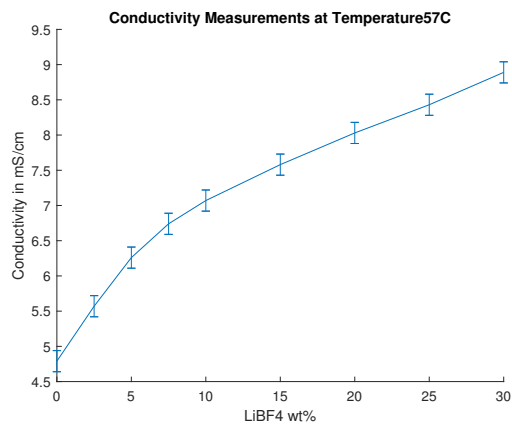


Figure A-14: Conductivity vs. wt% at a constant temperature of 57°C

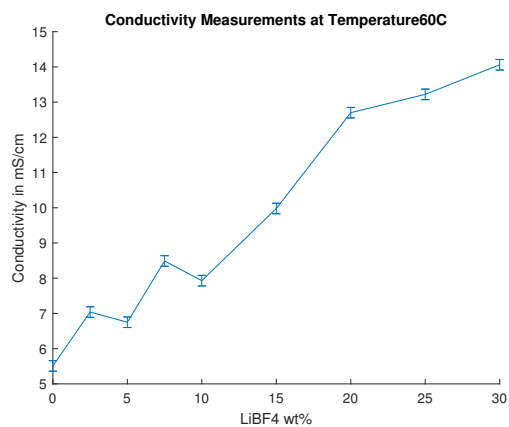


Figure A-15: Conductivity vs. wt% at a constant temperature of 60°C

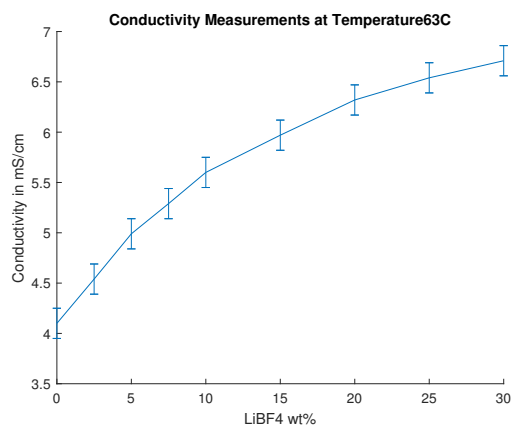


Figure A-16: Conductivity vs. wt% at a constant temperature of 63°C

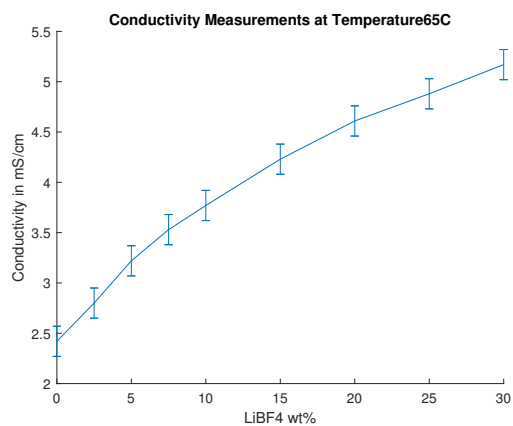


Figure A-17: Conductivity vs. wt% at a constant temperature of 65°C

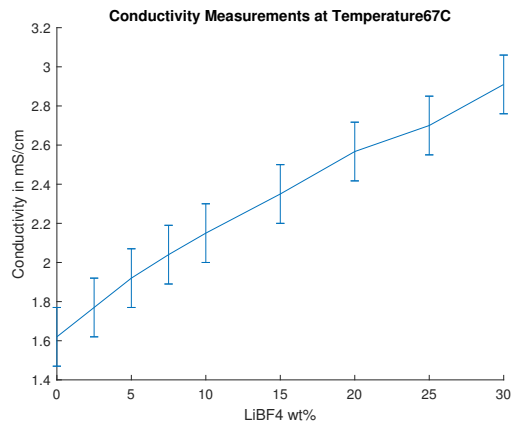


Figure A-18: Conductivity vs. wt% at a constant temperature of 67°C

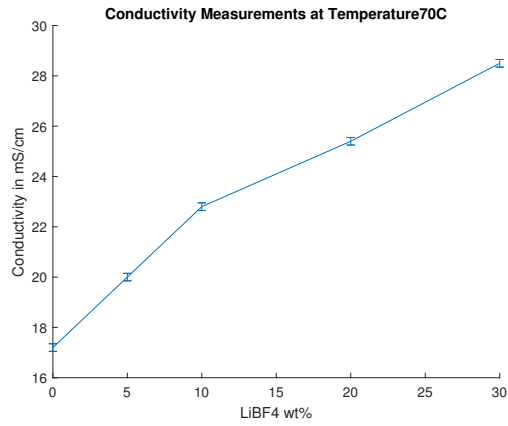


Figure A-19: Conductivity vs. wt% at a constant temperature of 70°C

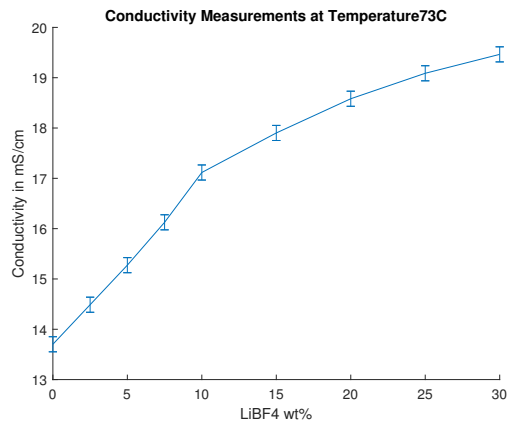


Figure A-20: Conductivity vs. wt% at a constant temperature of 73°C

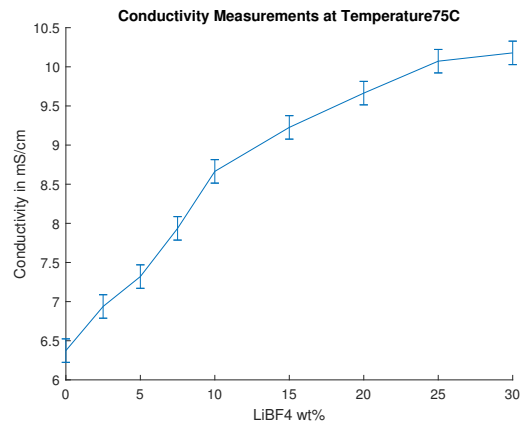


Figure A-21: Conductivity vs. wt% at a constant temperature of 75°C

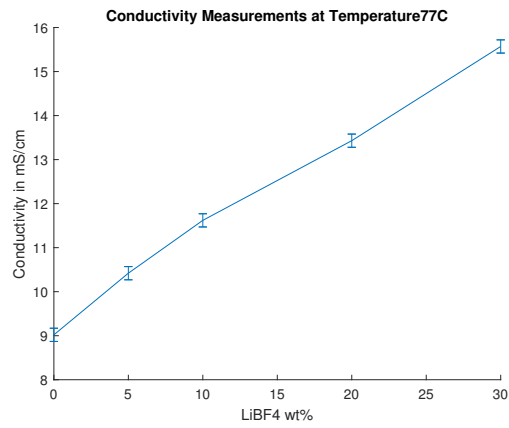


Figure A-22: Conductivity vs. wt% at a constant temperature of 77°C

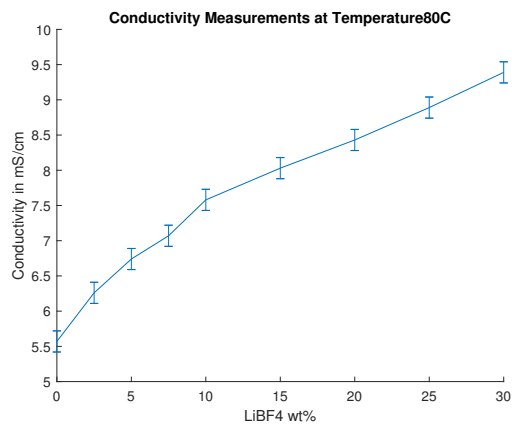


Figure A-23: Conductivity vs. wt% at a constant temperature of 80°C

Appendix B

Individual Conductivity vs. Temperature at constant wt% Graphs

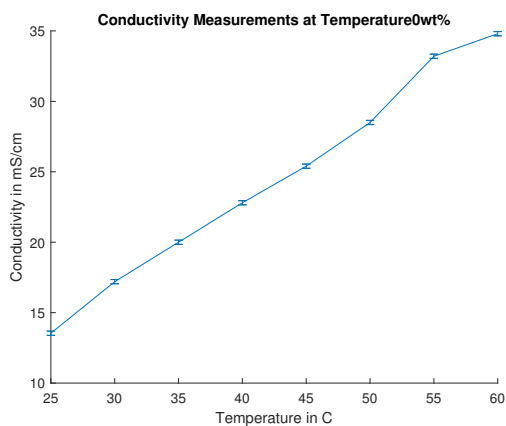


Figure B-1: Conductivity vs. T at a constant mixture with no $LiBF_4$ salt

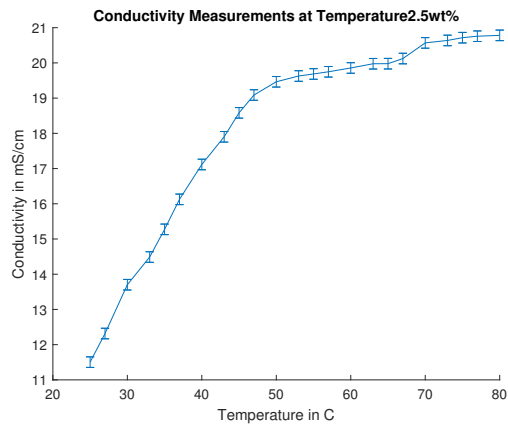


Figure B-2: Conductivity vs. T at a constant mixture with 2.5wt% of $LiBF_4$ salt.

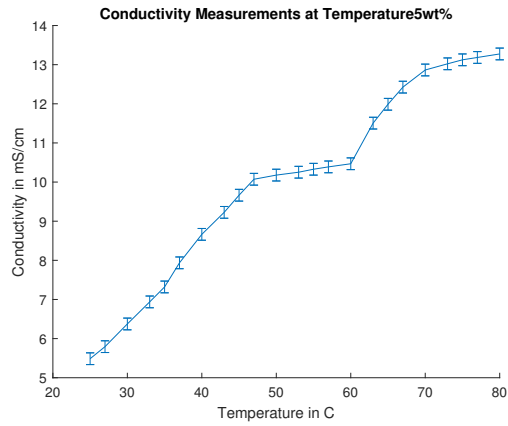


Figure B-3: Conductivity vs. T at a constant mixture with 5wt% of $LiBF_4$ salt.

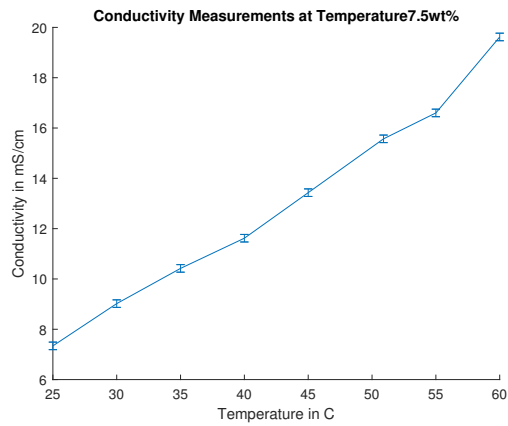


Figure B-4: Conductivity vs. T at a constant mixture with 7.5wt% of $LiBF_4$ salt.

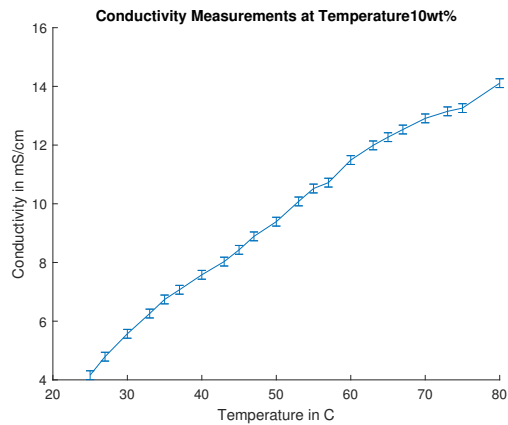


Figure B-5: Conductivity vs. T at a constant mixture with 10wt% of $LiBF_4$ salt.

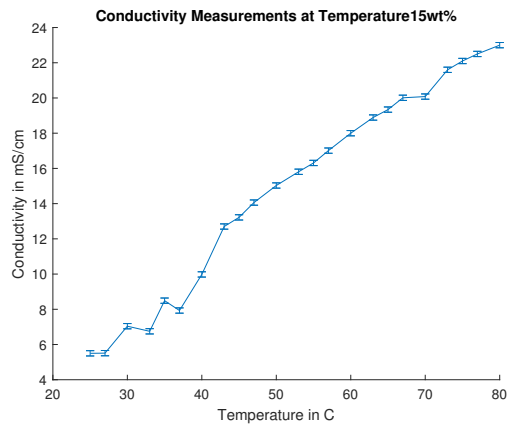


Figure B-6: Conductivity vs. T at a constant mixture with 15wt% of $LiBF_4$ salt.

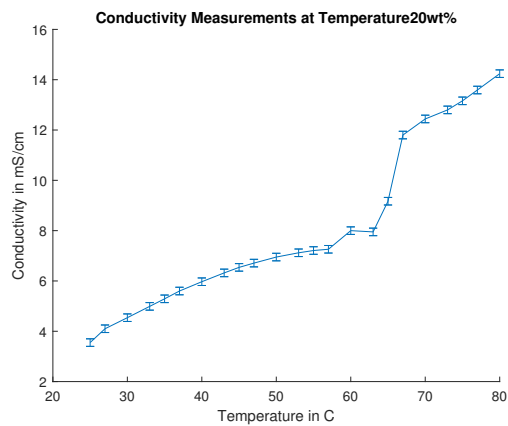


Figure B-7: Conductivity vs. T at a constant mixture with 20wt% of $LiBF_4$ salt.

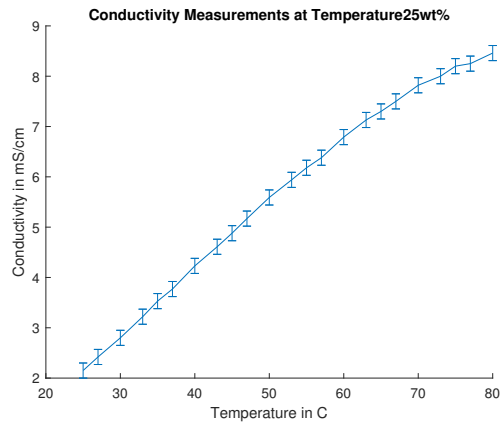


Figure B-8: Conductivity vs. T at a constant mixture with 25wt% of $LiBF_4$ salt.

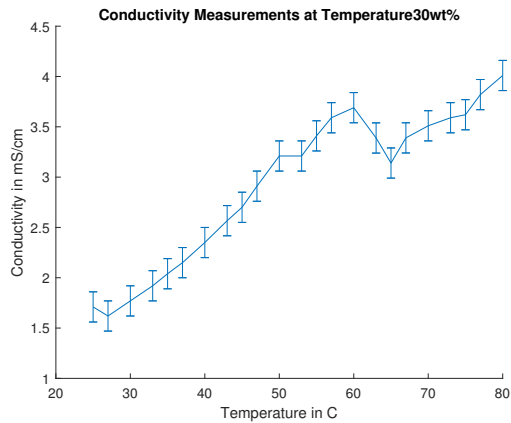


Figure B-9: Conductivity vs. T at a constant mixture with 30wt% of $LiBF_4$ salt.

Appendix C

Colour Changes Due To Temperature Experiments






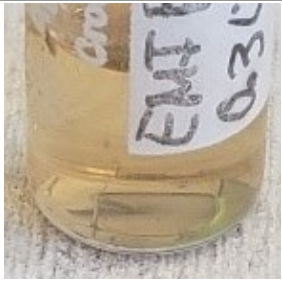
<i>wt%</i> of $LiBF_4$	Original Colour	Run 1	Run 3
5			
30			

Table C.1: Colour change after heating mixtures.

Bibliography

- [1] Caroline Lee Bates. Characterization of Fluorohydrogenated Ionic Liquids for Use in the Ion Electrospray Propulsion System, 2018.
- [2] Pierre Bonhôte, Ana Paula Dias, Nicholas Papageorgiou, Kuppaswamy Kalyanasundaram, and Michael Grätzel. Hydrophobic, Highly Conductive Ambient-Temperature Molten Salts. *Inorganic Chemistry*, 35(5):1168–1178, 1996.
- [3] Natalya Brikner and Paulo C. Lozano. The role of upstream distal electrodes in mitigating electrochemical degradation of ionic liquid ion sources. *Applied Physics Letters*, 101(19):7–10, 2012.
- [4] Thomas M. Coles and Paulo C. Lozano. Investigating efficiency losses from solvated ion fragmentation in electrospray thruster beams. *49th AIAA/ASME/SAE/ASEE Joint Propulsion Conference*, 1 PartF, 2013.
- [5] J. Fernández de la Mora and I. G. Loscertales. The current emitted by highly conducting Taylor cones. *Journal of Fluid Mechanics*, 260(special issue):155–184, 1994.
- [6] M. Gamero-Gastano and V. Hruby. Electrospray as a source of nanoparticles for efficient colloid thrusters. *36th AIAA/ASME/SAE/ASEE Joint Propulsion Conference and Exhibit*, 17(5), 2000.
- [7] Kikuko Hayamizu, Yuichi Aihara, Hiroe Nakagawa, Toshiyuki Nukuda, and William S. Price. Ionic conduction and ion diffusion in binary room-temperature ionic liquids composed of [emim][BF₄] and LiBF₄. *Journal of Physical Chemistry B*, 108(50):19527–19532, 2004.
- [8] J. G. Huddleston, A. E. Visser, W. M. Reichert, H. D. Willauer, G. A. Broker, and R. D. Rogers. Characterization and comparison of hydrophilic and hydrophobic room temperature ionic liquids incorporating the imidazolium cation. *Green Chemistry*, 3(4):156–164, 2001.
- [9] William Humphrey, Andrew Dalke, and Klaus Schulten. Vmd: Visual molecular dynamics. *Journal of Molecular Graphics*, 14(1):33 – 38, 1996.
- [10] William L. Jorgensen, David S. Maxwell, and Julian Tirado-Rives. Development and testing of the opls all-atom force field on conformational energetics

and properties of organic liquids. *Journal of the American Chemical Society*, 118(45):11225–11236, 1996.

- [11] Ha Na Kwon, Su Jin Jang, Yun Chan Kang, and Kwang Chul Roh. The effect of ILs as co-salts in electrolytes for high voltage supercapacitors. *Scientific Reports*, 9(1):1–6, 2019.
- [12] Zhe Li, Grant D Smith, and Dmitry Bedrov. Li, Smith, Bedrov - 2012 - Li solvation and transport properties in ionic liquidlithium salt mixtures a molecular dynamics simulation study.pdf. 2012.
- [13] K. N. Marsh, J. A. Boxall, and R. Lichtenthaler. Room temperature ionic liquids and their mixtures - A review. *Fluid Phase Equilibria*, 219(1):93–98, 2004.
- [14] Carla S Perez Martinez. Signature redacted -ct-e-d S ignatu Sig nature redacted Signature redacted. (2011), 2016.
- [15] N Mathews. VMD User ' s Guide. page 200, 2012.
- [16] Catherine E Miller. Characterization of Ion Cluster Fragmentation in Ionic Liquid Ion Sources. 2019.
- [17] C. S. Perez-Martinez and P. C. Lozano. Ion field-evaporation from ionic liquids infusing carbon xerogel microtips. *Applied Physics Letters*, 107(4):16–19, 2015.
- [18] Steve Plimpton. Short-Range Molecular Dynamics. *Journal of Computational Physics*, 117(6):1–42, 1997.
- [19] Benjamin D. Prince, Pavithra Tiruppathi, Raymond J. Bemish, Yu Hui Chiu, and Edward J. Maginn. Molecular Dynamics Simulations of 1-Ethyl-3-methylimidazolium Bis[(trifluoromethyl)sulfonyl]imide Clusters and Nanodrops. *Journal of Physical Chemistry A*, 119(2):352–368, 2015.
- [20] Hitoshi Shobukawa, Hiroyuki Tokuda, Sei Ichiro Tabata, and Masayoshi Watanabe. Preparation and transport properties of novel lithium ionic liquids. *Electrochimica Acta*, 50(2-3 SPEC. ISS.):305–309, 2004.
- [21] Alexander M. Smith and Susan Perkin. Influence of Lithium Solutes on Double-Layer Structure of Ionic Liquids. *Journal of Physical Chemistry Letters*, 6(23):4857–4861, 2015.
- [22] Nanako Takahashi. Molecular Dynamics Modeling of Ionic Liquids in Electro-spray Propulsion. 2010.
- [23] Geoffrey Taylor. Disintegration of water drops in an electric field. *Proceedings of the Royal Society of London. Series A, Mathematical and Physical Sciences*, 280(1382):383–397, 1964.
- [24] P Walden. Molecular weights and electrical conductivity of several fused salts. *Bull. Acad. Imper. Sci.*, pages 405–422, 1994.